FORCE schemes on unstructured meshes I: Conservative hyperbolic systems

Eleuterio F. Toro [a], Arturo Hidalgo [b], Michael Dumbser [a],*

[a] *Laboratory of Applied Mathematics, University of Trento, Via Mesiano 77, I-38100 Trento, Italy*
[b] *ETSI Minas, Universidad Politécnica de Madrid, Calle Ríos Rosas 21, E-28003 Madrid, Spain*

A B S T R A C T

This paper is about the construction of numerical fluxes of the centred type for one-step schemes in conservative form for solving general systems of conservation laws in multiple space dimensions on structured and unstructured meshes. The work is a multi-dimensional extension of the one-dimensional FORCE flux and is closely related to the work of Nessyahu–Tadmor and Arminjon. The resulting basic flux is first-order accurate and monotone; it is then extended to arbitrary order of accuracy in space and time on unstructured meshes in the framework of finite volume and discontinuous Galerkin methods. The performance of the schemes is assessed on a suite of test problems for the multi-dimensional Euler and Magnetohydrodynamics equations on unstructured meshes.

© 2009 Elsevier Inc. All rights reserved.

1. Introduction

The pioneering work of Lax and Wendroff [30], and more recently that of Hou and LeFloch [25], have established, theoretically, that numerical methods for systems of non-linear hyperbolic conservation laws must be conservative. Then, a key task is the prescription of monotone intercell numerical fluxes. These will then constitute the building block for a wide range of numerical methods constructed in the frameworks of finite volume and discontinuous Galerkin finite element methods, in either fully discrete or semi-discrete form, on structured or unstructured meshes. The construction of numerical fluxes has been a central research issue for over five decades, of which two very prominent and representative examples are the Lax–Friedrichs flux [29] and the Godunov flux [19]. These two methods introduced key ideas that have remained the pillars of current research. They are representative of the two distinct approaches for prescribing numerical fluxes, respectively termed *centred* (or symmetric) and *upwind* (or Riemann-problem based, or characteristic-based). Upwind schemes, explicitly use wave propagation information contained in the differential equations for the construction of the numerical flux, which is usually accomplished by solving a local one-dimensional Riemann problem, in the direction normal to a cell interface. The (classical) Riemann problem is the Cauchy problem for the relevant system of conservation laws along with piece-wise constant initial conditions, usually the cell averages on each side of the interface. Centred schemes, on the other hand, do not explicitly use wave propagation information contained in the corresponding Riemann problem. That is, centred schemes do

---

* Corresponding author. Tel.: +49 170 9360238; fax: +49 711 6856 3438.
E-mail addresses: toro@ing.unitn.it (E.F. Toro), arturo.hidalgo@upm.es (A. Hidalgo), michael.dumbser@ing.unitn.it (M. Dumbser).

not solve the Riemann problem in the conventional manner. However these schemes are not independent of the Riemann problem, as they use both the differential equations and the initial conditions of the Riemann problem.

This paper is about the construction of numerical fluxes of the centred type, for general hyperbolic systems in conservation-law form, in multiple space dimensions. The schemes are derived for Cartesian and non-Cartesian structured elements and for unstructured triangular and tetrahedral elements. A key ingredient of the present centred schemes is an averaging operator that results from the integral form of the conservation laws applied to appropriately chosen control volumes. Such operator is valid for both classical and weak solutions of conservations laws and is applicable to the one and the multidimensional cases. The present work builds upon two lines of current developments regarding centred methods. The first relates to the centred schemes reported by Nessyahu and Tadmor [35]. For extensions to unstructured meshes see the work of Arminjon and collaborators, e.g. [2], and for high order extensions see the work presented in [32,5,33]. The second line results from the FORCE scheme proposed by Toro and Billett [43]. As a matter of fact, the present work is a multi-dimensional extension of the FORCE scheme. Both approaches have the common feature of applying an averaging operator on staggered control volumes. In the Nessyahu–Tadmor approach the schemes consist of a two-step procedure on staggered grids and do not have a conservative form; in addition, the scheme is subject to a CFL restriction of 1/2. The FORCE scheme is a one-step procedure on a non-staggered grid and has a conservative form with a corresponding numerical flux, called the FORCE flux; it is subject to a CFL restriction of unity. The Nessyahu–Tadmor scheme is second-order accurate for smooth solutions and essentially non-oscillatory for discontinuous solutions, while the FORCE scheme is first-order accurate and monotone. The Nessyahu–Tadmor schemes have also been applied to multi-dimensional problems on regular Cartesian grids by Jiang and Tadmor [28], and to unstructured triangular and tetrahedral meshes by Arminjon and collaborators, see for example [2]. Available theoretical results for the Nessyahu–Tadmor schemes include proofs of convergence; Haasdonk et al. [21] proved convergence of the first-order version of the Nessyahu–Tadmor scheme for non-linear scalar conservation laws on unstructured triangular meshes. For the FORCE scheme convergence was proved by Chen and Toro [6] for the case of two non-linear systems of conservation laws in one space dimension, namely the isentropic equation of gas dynamics and the non-linear shallow water equations with a source term due to bed elevation.

In this paper we extend the FORCE approach to non-linear multi-dimensional systems of hyperbolic equations in conservation-law form. The schemes are one-step schemes in conservative form on unstaggered general meshes, where numerical fluxes emerge in a very natural way. Centred fluxes may be seen as being an appropriate solution of the Riemann problem without resolving the wave structure. For the purpose of analysis, FORCE schemes are also constructed on regular Cartesian meshes in two and three space dimensions. Various stencil configurations are explored and detailed analysis of monotonicity, linear stability and numerical viscosity is carried out. The most successful stencil configurations are extended to triangular meshes in two space dimensions and tetrahedral elements in three space dimensions.

The rest of the paper is structured as follows. Section 2 sets the background and reviews the FORCE and Nessyahu–Tadmor approaches, discussing common features and differences. In Section 3 we extend the FORCE approach and construct numerical fluxes for two and three dimensional general meshes; we also specialize the FORCE schemes to regular Cartesian meshes in two and three space dimensions for the purpose of analysis of the schemes. In Section 4 we extend the first-order monotone multidimensional FORCE schemes to arbitrary order of accuracy in both space and time following the ADER approach on unstructured meshes in two and three space dimensions (see, for instance [12,14,11]). In the same section we also compute convergence rates for smooth solutions. In Section 5 we assess the performance of the numerical schemes for shocked flows via a suite of test problems for the Euler and relativistic MHD equations. Conclusions are drawn in Section 6. In Appendix A and Appendix B we analyse the monotonicity, linear stability and numerical viscosity of the multidimensional FORCE schemes on Cartesian meshes.

2. Background

Here we review the one-dimensional FORCE flux in the framework of finite volume methods and discuss its relation with the Nessyahu–Tadmor approach.

2.1. The finite volume framework

We consider a one-dimensional system of m non-linear hyperbolic equations in conservation-law form

$$\partial_t \mathbf{Q} + \partial_x \mathbf{F}(\mathbf{Q}) = \mathbf{0}, \quad x \in \mathrm{R}, \quad t > 0, \tag{1}$$

where $\mathbf{Q}(x,t)$ is the vector of conserved variables and $\mathbf{F}(\mathbf{Q})$ is the vector of fluxes. We consider the Cauchy problem for (1) with initial condition of the form

$$\mathbf{Q}(x,t^n) = \mathbf{Q}^{(0)}(x). \tag{2}$$

Given the control volume $V \equiv \left[x_{i-\frac{1}{2}}, x_{i+\frac{1}{2}}\right] \times [t^n, t^{n+1}]$ of dimensions $\Delta t = t^{n+1} - t^n$ and $\Delta x = x_{i+\frac{1}{2}} - x_{i-\frac{1}{2}}$, one can integrate system (1) in space and time *exactly*, and divide by the cell width Δx to obtain the *averaging operator*

$$\frac{1}{\Delta x} \int_{x_{i-\frac{1}{2}}}^{x_{i+\frac{1}{2}}} \mathbf{Q}(x, t^{n+1}) dx = \frac{1}{\Delta x} \int_{x_{i-\frac{1}{2}}}^{x_{i+\frac{1}{2}}} \mathbf{Q}(x, t^n) - \frac{\Delta t}{\Delta x} \left[\frac{1}{\Delta t} \int_{t^n}^{t^{n+1}} \mathbf{F}\left(\mathbf{Q}\left(x_{i+\frac{1}{2}}, t\right)\right) dt - \frac{1}{\Delta t} \int_{t^n}^{t^{n+1}} \mathbf{F}\left(\mathbf{Q}\left(x_{i-\frac{1}{2}}, t\right)\right) dt \right]. \tag{3}$$

This operator defines an *average* of the solution of the Cauchy problem (1) at time $t = t^{n+1}$, for $x \in \left[x_{i-\frac{1}{2}}, x_{i+\frac{1}{2}} \right]$, requiring the spatial integration of the initial condition and the evaluation of the flux time integrals at $x = x_{i-\frac{1}{2}}$ and $x = x_{i+\frac{1}{2}}$. Eq. (3) can also be written as

$$\mathbf{Q}_i^{n+1} = \mathbf{Q}_i^n - \frac{\Delta t}{\Delta x} \left[\mathbf{F}_{i+\frac{1}{2}} - \mathbf{F}_{i-\frac{1}{2}} \right] \tag{4}$$

with the following definitions:

$$\mathbf{Q}_i^n = \frac{1}{\Delta x} \int_{x_{i-\frac{1}{2}}}^{x_{i+\frac{1}{2}}} \mathbf{Q}(x, t^n) dx, \quad \mathbf{F}_{i+\frac{1}{2}} = \frac{1}{\Delta t} \int_{t^n}^{t^{n+1}} \mathbf{F}\left(\mathbf{Q}\left(x_{i+\frac{1}{2}}, t \right) \right) dt. \tag{5}$$

Recall that the exact relation (4) gives rise to finite volume methods to solve (1) approximately in which $\mathbf{Q}_i^n$ and $\mathbf{F}_{i+\frac{1}{2}}$ are interpreted as approximations to the respective integrals (5).

2.2. Classical finite volume schemes

The Godunov approach [19] exploits the piece-wise constant distribution of the data $\mathbf{Q}_i^n$ and, locally, defines (classical) Riemann problems

$$\begin{aligned} &\text{PDEs}: \ \partial_t \mathbf{Q} + \partial_x \mathbf{F}(\mathbf{Q}) = \mathbf{0}, \\ &\text{IC}: \ \mathbf{Q}(x, 0) = \begin{cases} \mathbf{Q}_i^n & \text{if } x < 0, \\ \mathbf{Q}_{i+1}^n & \text{if } x > 0 \end{cases} \end{aligned} \tag{6}$$

with similarity solutions denoted by $\mathbf{Q}_{i+\frac{1}{2}}(x/t)$, where x and t are understood as local coordinates. Then the Godunov intercell numerical flux is

$$\mathbf{F}_{i+\frac{1}{2}} = \mathbf{F}(\mathbf{Q}_{i+\frac{1}{2}}(0)). \tag{7}$$

The solution $\mathbf{Q}_{i+\frac{1}{2}}(x/t)$ could be exact or approximate. In addition one could define approximations $\mathbf{F}_{i+\frac{1}{2}}$, directly, without requiring a state $\mathbf{Q}_{i+\frac{1}{2}}(x/t)$. For background on Godunov methods, see for example, [17,31,42]. Methods that explicitly exploit wave propagation information emanating from the solution of the Riemann problem are generally called *upwind* methods. The simplest upwind method is Rusanov's method [37], which only extracts an estimate for an upper bound for the maximum propagation speed in the local Riemann problem. One can define this scheme as a "one-wave solver". A two-wave solver is the HLL scheme [22], which requires estimates for lower and upper bounds for the speeds emanating from the local Riemann problem. We shall speak of a *complete* Riemann solver for the one whose wave model contains all m characteristic fields present in the exact solution. Otherwise, the Riemann solver will be termed *incomplete*.

It is possible to construct numerical fluxes $\mathbf{F}_{i+\frac{1}{2}}$, very approximately, without explicitly solving the Riemann problem (6), provided that what actually defines the Riemann problem is preserved, that is, the differential equations and the initial condition. Methods of this type include the so-called centred methods, or symmetric methods. Classical centred methods include the Lax–Wendroff method [30], the Lax–Friedrichs method [29] and the Godunov centred method [18], not to be mistaken with the Godunov upwind method.

The popular two-step version of the Lax–Wendroff method uses the averaging operator (3) in the control volume $[x_i, x_{i+1}] \times [t^n, t^n + \frac{1}{2}\Delta t]$ to obtain an integral average of the solution of the Riemann problem (6) at time $t^n + \frac{1}{2}\Delta t$, for $x \in [x_i, x_{i+1}]$ as follows:

$$\mathbf{Q}_{i+\frac{1}{2}}^{LW} = \frac{1}{2}(\mathbf{Q}_i^n + \mathbf{Q}_{i+1}^n) - \frac{1}{2} \frac{\Delta t}{\Delta x} [\mathbf{F}(\mathbf{Q}_{i+1}^n) - \mathbf{F}(\mathbf{Q}_i^n)]. \tag{8}$$

Then, the numerical flux is

$$\mathbf{F}_{i+\frac{1}{2}}^{LW} = \mathbf{F}(\mathbf{Q}_{i+\frac{1}{2}}^{LW}). \tag{9}$$

The Godunov centred method is analogous to the Lax–Wendroff method, it first computes an averaged state at the full time level

$$\mathbf{Q}_{i+\frac{1}{2}}^{GC} = \frac{1}{2}(\mathbf{Q}_i^n + \mathbf{Q}_{i+1}^n) - \frac{\Delta t}{\Delta x} [\mathbf{F}(\mathbf{Q}_{i+1}^n) - \mathbf{F}(\mathbf{Q}_i^n)], \tag{10}$$

and then computes the corresponding numerical flux as

$$\mathbf{F}_{i+\frac{1}{2}}^{GC} = \mathbf{F}\left(\mathbf{Q}_{i+\frac{1}{2}}^{GC} \right). \tag{11}$$

Compare the Godunov upwind flux (7) with the centred fluxes (9) and (11). Also, the classical Lax–Friedrichs method may be constructed with reference to the (staggered) Riemann problem

$$\text{PDEs}: \ \partial_t \mathbf{Q} + \partial_x \mathbf{F}(\mathbf{Q}) = \mathbf{0},$$

$$\text{IC}: \ \mathbf{Q}(x,0) = \begin{cases} \mathbf{Q}_{i-1}^n & \text{if } x_i < 0, \\ \mathbf{Q}_{i+1}^n & \text{if } x_i > 0. \end{cases} \tag{12}$$

One can define directly a cell average $\mathbf{Q}_i^{n+1}$ at the new time level for cell i as an average of the solution $\widehat{\mathbf{Q}}_i(x,t)$ of this Riemann problem at the half-time level, namely

$$\mathbf{Q}_i^{n+1} = \frac{1}{\Delta x} \int_{x_{i-\frac{1}{2}}}^{x_{i+\frac{1}{2}}} \widehat{\mathbf{Q}}_i \left(x, t^n + \frac{1}{2}\Delta t \right) dx. \tag{13}$$

Now, instead of solving the Riemann problem (12) to calculate (13) explicitly one applies the averaging operator to obtain

$$\mathbf{Q}_i^{n+1} = \frac{1}{2}(\mathbf{Q}_i^n + \mathbf{Q}_{i+1}^n) - \frac{1}{2}\frac{\Delta t}{\Delta x}[\mathbf{F}(\mathbf{Q}_{i+1}^n) - \mathbf{F}(\mathbf{Q}_i^n)], \tag{14}$$

which if written in conservative form (4) has numerical flux

$$\mathbf{F}_{i+\frac{1}{2}}^{LF} = \frac{1}{2}[\mathbf{F}(\mathbf{Q}_i^n) + \mathbf{F}(\mathbf{Q}_{i+1}^n)] - \frac{1}{2}\frac{\Delta x}{\Delta t}(\mathbf{Q}_{i+1}^n - \mathbf{Q}_i^n). \tag{15}$$

2.3. The FORCE scheme

The FORCE flux, first communicated in [41], was derived as a deterministic analogue of the staggered-grid version of Glimm's method [16], or Random Choice Method (RCM). This version of RCM advances the solution in two steps by randomly sampling exact solutions of Riemann problems using a staggered grid. The FORCE approach replaces randomly sampled exact solutions of classical (piece-wise constant data) Riemann problems in a two-stage procedure by an averaging operator at each stage. The end result is a deterministic one-step method, in conservative form, on a non-staggered grid, with a numerical flux, the FORCE flux. We note that there is a close relationship between the FORCE scheme and the scheme proposed earlier by Nessyahu and Tadmor [35], as we shall explain later.

Given the two local Riemann problem solutions $\mathbf{Q}_{i-\frac{1}{2}}(x/t)$ and $\mathbf{Q}_{i+\frac{1}{2}}(x/t)$, at the (local) time $t = \frac{1}{2}\Delta t$ we apply the averaging operator to obtain, respectively

$$\begin{aligned} \mathbf{Q}_{i-\frac{1}{2}}^{n+\frac{1}{2}} &= \frac{1}{2}(\mathbf{Q}_{i-1}^n + \mathbf{Q}_i^n) - \frac{1}{2}\frac{\Delta t}{\Delta x}[\mathbf{F}(\mathbf{Q}_i^n) - \mathbf{F}(\mathbf{Q}_{i-1}^n)], \\ \mathbf{Q}_{i+\frac{1}{2}}^{n+\frac{1}{2}} &= \frac{1}{2}(\mathbf{Q}_i^n + \mathbf{Q}_{i+1}^n) - \frac{1}{2}\frac{\Delta t}{\Delta x}[\mathbf{F}(\mathbf{Q}_{i+1}^n) - \mathbf{F}(\mathbf{Q}_i^n)]. \end{aligned} \tag{16}$$

The complete solution is restored back to the cell $I_i \equiv \left[x_{i-\frac{1}{2}}, x_{i+\frac{1}{2}} \right]$ in the second step by averaging the solution of the Riemann problem

$$\text{PDEs}: \ \partial_t \mathbf{Q} + \partial_x \mathbf{F}(\mathbf{Q}) = \mathbf{0},$$

$$\text{IC}: \ \mathbf{Q}(x,0) = \begin{cases} \mathbf{Q}_{i-\frac{1}{2}}^{n+\frac{1}{2}} & \text{if } x_i < 0, \\ \mathbf{Q}_{i+\frac{1}{2}}^{n+\frac{1}{2}} & \text{if } x_i > 0 \end{cases} \tag{17}$$

at time $t = \Delta t$, obtaining

$$\mathbf{Q}_i^{n+1} = \frac{1}{2}(\mathbf{Q}_{i-\frac{1}{2}}^{n+\frac{1}{2}} + \mathbf{Q}_{i+\frac{1}{2}}^{n+\frac{1}{2}}) - \frac{1}{2}\frac{\Delta t}{\Delta x}\left[\mathbf{F}\left(\mathbf{Q}_{i+\frac{1}{2}}^{n+\frac{1}{2}}\right) - \mathbf{F}(\mathbf{Q}_{i-\frac{1}{2}}^{n+\frac{1}{2}}) \right]. \tag{18}$$

The solution $\mathbf{Q}_i^{n+1}$ at the complete time step $t = \Delta t$ (globally, at time $t = t^n + \Delta t = t^{n+1}$) may now be expressed in terms of the conservative one-step formula (4), yielding, as a by product, the intercell numerical flux

$$\mathbf{F}_{i+\frac{1}{2}}^{FO} = \frac{1}{2}\left\{ \mathbf{F}\left(\mathbf{Q}_{i+\frac{1}{2}}^{n+\frac{1}{2}}\right) + \frac{1}{2}[\mathbf{F}(\mathbf{Q}_i^n) + \mathbf{F}(\mathbf{Q}_{i+1}^n)] - \frac{1}{2}\frac{\Delta x}{\Delta t}(\mathbf{Q}_{i+1}^n - \mathbf{Q}_i^n) \right\} \tag{19}$$

called the FORCE flux. It turns out that this flux is in fact the mean between the two-step version of the Lax–Wendroff flux (9) and the Lax–Friedrichs flux (15), that is

$$\mathbf{F}_{i+\frac{1}{2}}^{FO} = \frac{1}{2}\left(\mathbf{F}_{i+\frac{1}{2}}^{LW} + \mathbf{F}_{i+\frac{1}{2}}^{LF} \right). \tag{20}$$

We also recall some basic properties of FORCE and related schemes in terms of the model hyperbolic equation

$$\partial_t q(x,t) + \lambda \partial_x q(x,t) = 0, \quad \lambda: \ \text{constant}. \tag{21}$$

Table 1 summarizes the results, where $c = \frac{\lambda \Delta t}{\Delta x}$ is the Courant number. Note that the first-order Godunov centred scheme is not monotone in its full range of linear stability. The FORCE scheme, as the classical Lax–Friedrichs scheme, is monotone in its full range of linear stability.

Table 1
Accuracy, linear stability and monotonicity of selected schemes.

	Accuracy	Linear stability	Monotonicity
Godunov upwind	First-order	$0 \leqslant |c| \leqslant 1$	Yes
Lax–Wendroff	Second-order	$0 \leqslant |c| \leqslant 1$	No
Godunov centred	First-order	$0 \leqslant |c| \leqslant \frac{1}{2}\sqrt{2}$	Not for $0 \leqslant |c| \leqslant \frac{1}{2}$
Lax–Friedrichs	First-order	$0 \leqslant |c| \leqslant 1$	Yes
FORCE	First-order	$0 \leqslant |c| \leqslant 1$	Yes

For more properties of the FORCE flux see [43]. See also [6], where the scheme is shown to be convergent for the non-linear shallow water equations and for isentropic gas dynamics.

Modern numerical methods for hyperbolic conservation laws are, first of all, conservative. This requires a numerical flux. If first-order of accuracy is regarded as sufficient, then the numerical flux must be monotone (for the scalar case). If high accuracy, ideally in both space and time, is desirable, for smooth solutions, then the schemes must also be free from spurious oscillations in the vicinity of large gradients, shock waves in particular. But according to Godunov's theorem [19], these two requirements are contradictory, for linear schemes. The only way out is to construct non-linear schemes. These are based on two basic building blocks: non-linear spatial reconstruction operators and a basic first-order *monotone* flux. From this point of view, the only useful schemes from Table 1 are the Godunov upwind, Lax–Friedrichs and the FORCE schemes. However, it is known that it is not possible to construct second-order TVD schemes based on the Lax–Friedrichs scheme, as reported in [43], leaving the Godunov upwind scheme and the FORCE scheme. The former resolves more fully the Riemann problem and the latter approximates the solution of the Riemann problem by a combination of averages.

2.4. The Nessyahu–Tadmor scheme

The Nessyahu and Tadmor approach [35] in one space dimension considers a sequence of generalized (non classical) Riemann problems, whose initial conditions are given by piece-wise non-linear reconstructions of first degree polynomials. Then the averaging operator is applied in a two-step, staggered-grid fashion. In the first step one considers the Riemann problem

$$\text{PDEs}: \ \partial_t \mathbf{Q} + \partial_x \mathbf{F}(\mathbf{Q}) = \mathbf{0},$$
$$\text{IC}: \ \mathbf{Q}(x,0) = \begin{cases} \mathbf{P}_i(x) = \mathbf{Q}_i^n + (x - x_i)\Delta_i & \text{if } x < x_{i+\frac{1}{2}}, \\ \mathbf{P}_{i+1}(x) = \mathbf{Q}_{i+1}^n + (x - x_{i+1})\Delta_{i+1} & \text{if } x > x_{i+\frac{1}{2}}, \end{cases} \tag{22}$$

where Δ_i is a vector of suitable slopes, chosen so as to control spurious oscillations. Applying the averaging operator (3) in the control volume $[x_i, x_{i+1}] \times [t^n, t^n + \delta t]$ one obtains an integral average of the solution at time $t^n + \delta t$, for $x \in [x_i, x_{i+1}]$, as follows:

$$\widehat{\mathbf{Q}}_{i+\frac{1}{2}} = \frac{1}{2}(\mathbf{Q}_i^n + \mathbf{Q}_{i+1}^n) - \frac{1}{8}\Delta x(\Delta_i - \Delta_{i+1}) - \left[\frac{1}{\delta t} \int_{t^n}^{t^n + \delta t} \mathbf{F}(\mathbf{Q}(x_{i+1}, t))dt - \frac{1}{\delta t} \int_{t^n}^{t^n + \delta t} \mathbf{F}(\mathbf{Q}(x_i, t))dt \right]. \tag{23}$$

The fluxes are computed by a mid-point rule approximation to the time integrals. For example, for the flux at x_i the Nessyahu–Tadmor approach proceeds as follows. By means of the Cauchy–Kowalewski method one obtains, at x_i, a state $\widehat{\mathbf{Q}}_i$ given as

$$\widehat{\mathbf{Q}}_i = \mathbf{Q}_i^n + \frac{1}{2}\delta t \partial_t \mathbf{Q}_i^n = \mathbf{Q}_i^n - \frac{1}{2}\delta t \partial_x \mathbf{F}(\mathbf{Q}_i^n). \tag{24}$$

Then the required flux approximation is

$$\widehat{\mathbf{F}}_i = \mathbf{F}(\widehat{\mathbf{Q}}_i). \tag{25}$$

An analogous procedure is applied at x_{i+1}. For the second step of the method one has the set of cell averages $\{\widehat{\mathbf{Q}}_{i+\frac{1}{2}}\}$ at the interfaces. Again, a reconstruction operator is applied and a generalized Riemann problem

$$\text{PDEs}: \ \partial_t \mathbf{Q} + \partial_x \mathbf{F}(\mathbf{Q}) = \mathbf{0},$$
$$\text{IC}: \ \mathbf{Q}(x,0) = \begin{cases} \widehat{\mathbf{P}}_{i-\frac{1}{2}}(x) = \widehat{\mathbf{Q}}_{i-\frac{1}{2}} + \left(x - x_{i-\frac{1}{2}}\right)\widehat{\Delta}_{i-\frac{1}{2}} & \text{if } x < x_i, \\ \widehat{\mathbf{P}}_{i+\frac{1}{2}}(x) = \widehat{\mathbf{Q}}_{i+\frac{1}{2}} + \left(x - x_{i+\frac{1}{2}}\right)\widehat{\Delta}_{i+\frac{1}{2}} & \text{if } x > x_i \end{cases} \tag{26}$$

is considered. Applying the averaging operator (3) in the control volume $[x_{i-\frac{1}{2}}, x_{i+\frac{1}{2}}] \times [t^n + \delta t, t^n + \delta t + \widehat{\delta t}]$ one obtains an integral average of the solution of the Riemann problem (26) at time $t^n + \delta t + \widehat{\delta t}$, for $x \in \left[x_{i-\frac{1}{2}}, x_{i+\frac{1}{2}}\right]$, completing the solution procedure after a time $\Delta t = \delta t + \widehat{\delta t}$, restoring solution values back to the centres of the volumes.

Remarks on the FORCE and Nessyahu–Tadmor schemes: First we note that none of the methods discussed so far can escape the Riemann problem. Upwind methods resolve, exactly or approximately, the details of the wave structure emanating from the interface. Instead, the so-called centred methods, using the integral form of the conservation laws, average the solution of the Riemann problem in appropriately chosen control volumes. The Nessyahu–Tadmor scheme averages solutions of generalized Riemann problems, resulting in a second-order accurate scheme, for smooth solutions, and essentially non-oscillatory at shocks, which requires non-linear reconstructions twice, one in each sub-step. Moreover, each sub-step is subject to the CFL restriction $C_{cfl} \leqslant 1/2$ and the time steps δt and $\widehat{\delta t}$ are not necessarily related. We note also that the stencil of the complete Nessyahu–Tadmor scheme has 6 points, in contrast to most one-step TVD methods.

The relationship between the FORCE and the Nessyahu–Tadmor schemes can be summarized as follows: the former can be obtained from the latter if the following conditions were observed: (i) no reconstruction in the Nessyahu–Tadmor scheme, (ii) $\delta t = \widehat{\delta t} = \frac{1}{2} \Delta t$ imposed, (iii) algebraic manipulations performed so as to end up with a one-step conservative scheme, with a corresponding numerical flux.

The next section addresses the first main point of this paper, which is the construction of a multi-dimensional version of the FORCE scheme that is applicable to general meshes in two and three space dimensions.

3. FORCE schemes in multiple space dimensions

Consider a general system of non-linear conservation laws in α space dimensions

$$\partial_t \mathbf{Q} + \mathrm{div}(\underline{\underline{\mathbf{F}}}(\mathbf{Q})) = \mathbf{0}, \tag{27}$$

where $\underline{\underline{\mathbf{F}}} = (f(\mathbf{Q}), g(\mathbf{Q}), h(\mathbf{Q}))$ is the flux tensor.

We first construct the schemes in the setting of general meshes and later, for the purpose of analysis of the schemes, we specialize the approach to Cartesian meshes in two and three space dimensions.

3.1. FORCE schemes on general meshes

We assume a conforming tessellation $\mathcal{T}_\Omega$ of the computational domain $\Omega \subset \mathrm{R}^\alpha$ by elements T_i such that

$$\mathcal{T}_\Omega = \bigcup_i T_i. \tag{28}$$

Each element T_i has n_f plane faces ∂T_i^j of area S_j, with associated outward pointing face-normal vectors $\vec{n}_j$. The total volume $|T_i|$ of element T_i is sub-divided into sub-volumes V_j^- generated by connecting the barycentre of element T_i with the vertices of face j. The corresponding adjacent sub-volume in the neighboring element that shares face ∂T_i^j with element T_i is denoted as V_j^+. Fig. 1 illustrates the above definitions and notation for the two-dimensional case. Note that the intersection of V_j^- and V_j^+ gives the edge j of the element T_i. With reference to Fig. 1 we distinguish two kinds of elements: *primary elements* T_i, at which the solution is sought at each time step, and *secondary elements* formed by $V_j^- \bigcup V_j^+$, for $j = 1, 2, 3$. Obviously, the sub-volumes $|V_j^-|$ add up to the total volume of T_i, that is

$$|T_i| = \sum_{j=1}^{n_f} |V_j^-|. \tag{29}$$

Now, an extension of the averaging operator (3) is obtained by integrating the conservation law (27) over a space-time control volume $T_i \times [t^n, t^{n+1}]$, namely
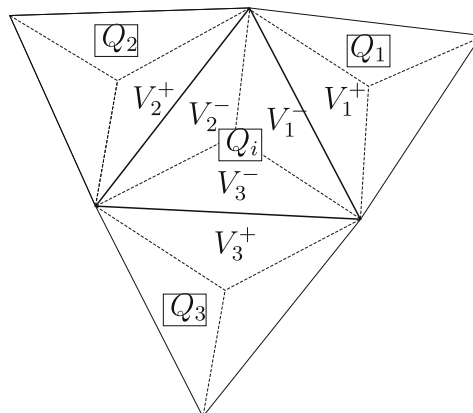

Fig. 1. Notation for a general configuration on an unstructured triangular mesh.

$$\mathbf{Q}_i^{n+1} = \mathbf{Q}_i^n - \frac{\Delta t}{|T_i|} \sum_{j=1}^{n_f} \int_{\partial T_i^j} \underline{\underline{\mathbf{F}}}(\mathbf{Q}) \cdot \vec{n}_j \, dS, \tag{30}$$

where $\mathbf{Q}_i^n$ is the cell average at time level n and $\Delta t = t^{n+1} - t^n$ is the time step.

Our multi-dimensional extension of the FORCE flux on unstructured meshes is now obtained as follows: first, assuming averages in each *primary elements* at time $t = t^n$ we obtain an averaged state for each face ∂T_i^j at the half-time level $t^{n+\frac{1}{2}} = t^n + \frac{1}{2}\Delta t$, by integrating the conservation laws (27) over the the *secondary elements*, that is the space-time control volume $\{V_j^- \cup V_j^+\} \times \left[t^n, t^{n+1}\right]$. The averaged state at the half-time level on each face ∂T_i^j is given by

$$\mathbf{Q}_{j+\frac{1}{2}}^{n+\frac{1}{2}} = \frac{\mathbf{Q}_i^n V_j^- + \mathbf{Q}_j^n V_j^+}{V_j^- + V_j^+} - \frac{1}{2} \frac{\Delta t S_j}{V_j^- + V_j^+} (\underline{\underline{\mathbf{F}}}(\mathbf{Q}_j^n) - \underline{\underline{\mathbf{F}}}(\mathbf{Q}_i^n)) \cdot \vec{n}_j. \tag{31}$$

With these initial conditions at time $t^{n+\frac{1}{2}} = t^n + \frac{1}{2}\Delta t$, by averaging over the *primary elements* $T_i \times \left[t^{n+\frac{1}{2}}, t^{n+1}\right]$ yields averages at time $t^{n+1} = t^n + \Delta t$, namely

$$\mathbf{Q}_i^{n+1} = \frac{1}{|T_i|} \sum_{j=1}^{n_f} \left(\mathbf{Q}_{j+\frac{1}{2}}^{n+\frac{1}{2}} V_j^- - \frac{1}{2} \Delta t S_j \underline{\underline{\mathbf{F}}}\left(\mathbf{Q}_{j+\frac{1}{2}}^{n+\frac{1}{2}}\right) \cdot \vec{n}_j \right). \tag{32}$$

Eqs. (31) and (32) constitute a first-order accurate, explicit two-step method for solving (27) on a staggered mesh. Following the FORCE approach [43], this scheme can now be written as a one-step scheme in conservative form on a non-staggered mesh, with a corresponding numerical flux. After some algebraic manipulations involving Gauss' theorem ($\sum_j S_j \vec{n}_j = 0$) and normalizing the face-normal vectors ($\vec{n}_j^2 = 1$), we can recast the scheme (31) and (32) into the sought conservative form

$$\mathbf{Q}_i^{n+1} = \mathbf{Q}_i^n - \frac{\Delta t}{|T_i|} \sum_{j=1}^{n_f} S_j \underline{\underline{\mathbf{F}}}_{j+\frac{1}{2}}^{\text{FORCE}\alpha} \cdot \vec{n}_j, \tag{33}$$

where the resulting FORCE flux for general meshes in multiple space dimensions, called FORCEα in the following, is defined as

$$\underline{\underline{\mathbf{F}}}_{j+\frac{1}{2}}^{\text{FORCE}\alpha} = \frac{1}{2} \left(\underline{\underline{\mathbf{F}}}_{j+\frac{1}{2}}^{LW\alpha}\left(\mathbf{Q}_i^n, \mathbf{Q}_j^n\right) + \underline{\underline{\mathbf{F}}}_{j+\frac{1}{2}}^{LF\alpha}\left(\mathbf{Q}_i^n, \mathbf{Q}_j^n\right) \right). \tag{34}$$

The FORCE flux on general meshes in multiple space dimensions is then the arithmetic average of two fluxes: a two-point flux of the Lax–Wendroff type and a two-point flux of the Lax–Friedrichs type. These two component fluxes appear to be new and are natural generalizations of the one-dimensional Lax–Wendroff and Lax–Friedrichs fluxes to general meshes in multiple space dimensions. The Lax–Wendroff type flux is given by the physical flux $\underline{\underline{\mathbf{F}}}$ evaluated at the intermediate state obtained from the first averaging procedure (31):

$$\underline{\underline{\mathbf{F}}}_{j+\frac{1}{2}}^{LW\alpha}\left(\mathbf{Q}_i^n, \mathbf{Q}_j^n\right) = \underline{\underline{\mathbf{F}}}\left(\mathbf{Q}_{j+\frac{1}{2}}^{n+\frac{1}{2}}\right), \tag{35}$$

$$\mathbf{Q}_{j+\frac{1}{2}}^{n+\frac{1}{2}} = \frac{\mathbf{Q}_i^n V_j^- + \mathbf{Q}_j^n V_j^+}{V_j^- + V_j^+} - \frac{1}{2} \frac{\Delta t S_j}{V_j^- + V_j^+} \left(\underline{\underline{\mathbf{F}}}\left(\mathbf{Q}_j^n\right) - \underline{\underline{\mathbf{F}}}\left(\mathbf{Q}_i^n\right) \right) \cdot \vec{n}_j. \tag{36}$$

The Lax–Friedrichs-type flux for general meshes in multiple space dimensions is defined as follows:

$$\underline{\underline{\mathbf{F}}}_{j+\frac{1}{2}}^{LF\alpha}\left(\mathbf{Q}_i^n, \mathbf{Q}_j^n\right) = \frac{V_j^- \underline{\underline{\mathbf{F}}}\left(\mathbf{Q}_j^n\right) + V_j^+ \underline{\underline{\mathbf{F}}}(\mathbf{Q}_i^n)}{V_j^- + V_j^+} - \frac{V_j^- V_j^+}{V_j^- + V_j^+} \frac{2}{\Delta t S_j} \left(\mathbf{Q}_j^n - \mathbf{Q}_i^n\right) \vec{n}_j^T. \tag{37}$$

Using these generalized Lax–Wendroff and Lax–Friedrichs fluxes we will also consider a further generalization of the multi-dimensional FORCE flux obtained as the weighted average ($0 \leqslant \omega \leqslant 1$) of these two fluxes, namely

$$\underline{\underline{\mathbf{F}}}_{j+\frac{1}{2}}^{\text{GFORCE}\alpha} = \omega \underline{\underline{\mathbf{F}}}_{j+\frac{1}{2}}^{LW\alpha}\left(\mathbf{Q}_i^n, \mathbf{Q}_j^n\right) + (1 - \omega) \underline{\underline{\mathbf{F}}}_{j+\frac{1}{2}}^{LF\alpha}\left(\mathbf{Q}_i^n, \mathbf{Q}_j^n\right). \tag{38}$$

This will be called the GFORCEα flux and is a straight generalization of the one-dimensional GFORCE scheme. In the next section we study two-dimensional and three-dimensional FORCE schemes on Cartesian meshes.

3.2. FORCE schemes on Cartesian meshes

Here, for the purpose of analysis, we apply the FORCE scheme in Cartesian meshes, in two and three space dimensions. Recall that the FORCE approach consists of identifying primary and secondary volumes or elements, application of an averaging operator on each type of control volumes in succession and recovery of the conservation form of the scheme, with an appropriate numerical flux. The primary volumes are perfectly Cartesian squares in two dimensions and cubes in three dimensions. As secondary volumes we consider two choices: edge-based secondary volumes and vertex-based secondary volumes. We study monotonicity, linear stability and numerical viscosity of the resulting schemes.

3.2.1. FORCE scheme on edge-based secondary volumes

Fig. 2 illustrates the primary volumes and secondary volumes for the two-dimensional Cartesian mesh case. Here, in the first step of the scheme one chooses *edge-based* secondary volumes. FORCE schemes on uniform Cartesian meshes in α dimensions can be derived from Eqs. (34)–(37) as special cases. In one space dimension the secondary volumes are $V_j^+ = V_j^- = \frac{1}{2}\Delta x$ and the face surface area is $S_j = 1$. In two space dimensions we have the secondary volumes $V_j^+ = V_j^- = \frac{1}{4}\Delta x^2$ and the face surface $S_j = \Delta x$. Finally, in three space dimensions we get $V_j^+ = V_j^- = \frac{1}{6}\Delta x^3$ for the secondary volumes and $S_j = \Delta x^2$ for the face surface. This leads to the following Cartesian versions of the multi-dimensional FORCE fluxes, which are still averages of Lax–Wendroff type and Lax–Friedrichs type fluxes. The flux in the x-direction is

$$\mathbf{F}_{i+\frac{1}{2}}^{\text{FORCE}} = \frac{1}{2}\left(\mathbf{F}_{i+\frac{1}{2}}^{LW\alpha} + \mathbf{F}_{i+\frac{1}{2}}^{LF\alpha}\right) \tag{39}$$

with

$$\mathbf{F}_{i+\frac{1}{2}}^{LW\alpha} = \mathbf{F}\left(\mathbf{Q}_{j+\frac{1}{2}}^{n+\frac{1}{2}}\right), \tag{40}$$

$$\mathbf{Q}_{j+\frac{1}{2}}^{n+\frac{1}{2}} = \frac{1}{2}\left(\mathbf{Q}_i^n + \mathbf{Q}_{i+1}^n\right) - \frac{1}{2}\frac{\alpha\Delta t}{\Delta x}\left(\mathbf{F}(\mathbf{Q}_{i+1}^n) - \mathbf{F}(\mathbf{Q}_i^n)\right) \tag{41}$$

and

$$\mathbf{F}_{i+\frac{1}{2}}^{LF\alpha} = \frac{1}{2}\left(\mathbf{F}(\mathbf{Q}_{i+1}^n) + \mathbf{F}(\mathbf{Q}_i^n)\right) - \frac{1}{2}\frac{\Delta x}{\alpha\Delta t}\left(\mathbf{Q}_{i+1}^n - \mathbf{Q}_i^n\right). \tag{42}$$

The fluxes in the other Cartesian directions have analogous form and are not reproduced here. There are two classes of numerical methods associated with the generalized Lax–Wendroff (40) and generalized Lax–Friedrichs (42) fluxes. For each value of the dimension parameter α there corresponds a numerical scheme. The case $\alpha = 2$ gives a generalized Lax–Wendroff flux that is not new; it is in fact identical to the Godunov centred flux. The generalized Lax–Friedrichs schemes for $\alpha = 2$ appears to be new. In fact we have studied in detail the properties of the one-dimensional schemes corresponding to the generalized Lax–Wendroff and generalized Lax–Friedrichs schemes, regarding the dimension α a parameter open to choice. The results are omitted.

3.2.2. FORCE scheme on vertex-based secondary volumes

Here we keep the perfectly Cartesian *primary volumes* $C_{i,j}$ of area Δx^2, as previously, but as secondary volumes we choose vertex-based control volumes. This stencil was considered by Jiang and Tadmor [28]. In the first step the averaging operator is applied to perfectly squared *secondary volumes* of area Δx^2 around each of the four vertexes of a given primary cell $C_{i,j}$, with initial conditions at time $t = t^n$. In the second step the averaging is applied inside the primary cell $C_{i,j}$ with initial conditions obtained from the first step. The four vertices of cell $C_{i,j}$ are denoted by $(i-\frac{1}{2}, j-\frac{1}{2})$, $(i+\frac{1}{2}, j-\frac{1}{2})$, $(i+\frac{1}{2}, j+\frac{1}{2})$, $(i-\frac{1}{2}, j+\frac{1}{2})$. The first step applied to the vertex-based secondary volumes gives
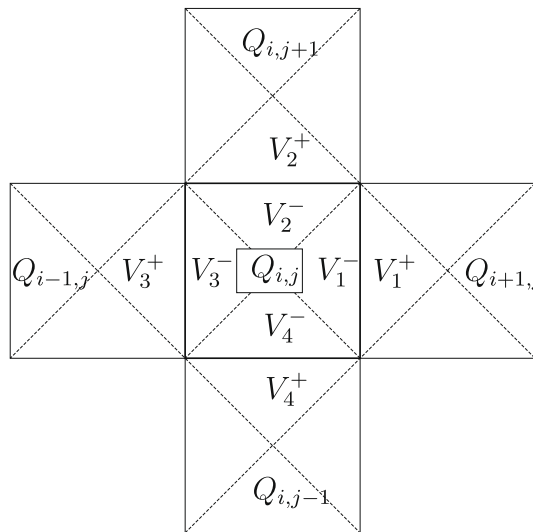

Fig. 2. Primary and secondary control volumes for the FORCE scheme on a regular Cartesian grid in two space dimensions. The secondary volumes are edge-based.

$$\mathbf{Q}_{i-\frac{1}{2}j-\frac{1}{2}}^{n+\frac{1}{2}} = \frac{1}{4}\left(\mathbf{Q}_{i-1j-1}^{n} + \mathbf{Q}_{ij-1}^{n} + \mathbf{Q}_{ij}^{n} + \mathbf{Q}_{i-1j}^{n}\right) - \frac{1}{4}\frac{\Delta t}{\Delta x}\left[\mathbf{F}_{ij-1}^{n} - \mathbf{F}_{i-1j-1}^{n} + \mathbf{F}_{ij}^{n} - \mathbf{F}_{i-1j}^{n} + \mathbf{G}_{i-1j}^{n} - \mathbf{G}_{i-1j-1}^{n} + \mathbf{G}_{ij}^{n} - \mathbf{G}_{ij-1}^{n}\right], \quad (43)$$

$$\mathbf{Q}_{i+\frac{1}{2}j-\frac{1}{2}}^{n+\frac{1}{2}} = \frac{1}{4}\left(\mathbf{Q}_{ij-1}^{n} + \mathbf{Q}_{i+1j-1}^{n} + \mathbf{Q}_{i+1j}^{n} + \mathbf{Q}_{ij}^{n}\right) - \frac{1}{4}\frac{\Delta t}{\Delta x}\left[\mathbf{F}_{i+1j-1}^{n} - \mathbf{F}_{ij-1}^{n} + \mathbf{F}_{i+1j}^{n} - \mathbf{F}_{ij}^{n} + \mathbf{G}_{i+1j}^{n} - \mathbf{G}_{i+1j-1}^{n} + \mathbf{G}_{ij}^{n} - \mathbf{G}_{ij-1}^{n}\right], \quad (44)$$

$$\mathbf{Q}_{i+\frac{1}{2}j+\frac{1}{2}}^{n+\frac{1}{2}} = \frac{1}{4}\left(\mathbf{Q}_{ij}^{n} + \mathbf{Q}_{i+1j}^{n} + \mathbf{Q}_{i+1j+1}^{n} + \mathbf{Q}_{ij+1}^{n}\right) - \frac{1}{4}\frac{\Delta t}{\Delta x}\left[\mathbf{F}_{i+1j}^{n} - \mathbf{F}_{ij}^{n} + \mathbf{F}_{i+1j+1}^{n} - \mathbf{F}_{ij+1}^{n} + \mathbf{G}_{i+1j+1}^{n} - \mathbf{G}_{i+1j}^{n} + \mathbf{G}_{ij+1}^{n} - \mathbf{G}_{ij}^{n}\right], \quad (45)$$

$$\mathbf{Q}_{i-\frac{1}{2}j+\frac{1}{2}}^{n+\frac{1}{2}} = \frac{1}{4}\left(\mathbf{Q}_{ij}^{n} + \mathbf{Q}_{ij+1}^{n} + \mathbf{Q}_{i-1j+1}^{n} + \mathbf{Q}_{i-1j}^{n}\right) - \frac{1}{4}\frac{\Delta t}{\Delta x}\left[\mathbf{F}_{ij}^{n} - \mathbf{F}_{i-1j}^{n} + \mathbf{F}_{ij+1}^{n} - \mathbf{F}_{i-1j+1}^{n} + \mathbf{G}_{ij+1}^{n} - \mathbf{G}_{ij}^{n} + \mathbf{G}_{i-1j+1}^{n} - \mathbf{G}_{i-1j}^{n}\right]. \quad (46)$$

The second step applied to the primary volume C_{ij} with initial conditions at time $t = t^n + \frac{1}{2}\Delta t$ gives the solution at time $t = t^{n+1} = t^n + \Delta t$ in the primary volume C_{ij} as

$$\mathbf{Q}_{ij}^{n+1} = \frac{1}{4}\left(\mathbf{Q}_{i-\frac{1}{2}j-\frac{1}{2}}^{n+\frac{1}{2}} + \mathbf{Q}_{i+\frac{1}{2}j-\frac{1}{2}}^{n+\frac{1}{2}} + \mathbf{Q}_{i+\frac{1}{2}j+\frac{1}{2}}^{n+\frac{1}{2}} + \mathbf{Q}_{i-\frac{1}{2}j+\frac{1}{2}}^{n+\frac{1}{2}}\right) - \frac{1}{4}\frac{\Delta t}{\Delta x}\left[\mathbf{F}_{i+\frac{1}{2}j-\frac{1}{2}}^{n+\frac{1}{2}} + \mathbf{F}_{i+\frac{1}{2}j+\frac{1}{2}}^{n+\frac{1}{2}} - \mathbf{F}_{i-\frac{1}{2}j-\frac{1}{2}}^{n+\frac{1}{2}} - \mathbf{F}_{i-\frac{1}{2}j+\frac{1}{2}}^{n+\frac{1}{2}}\right]$$
$$- \frac{1}{4}\frac{\Delta t}{\Delta x}\left[\mathbf{G}_{i-\frac{1}{2}j+\frac{1}{2}}^{n+\frac{1}{2}} + \mathbf{G}_{i+\frac{1}{2}j+\frac{1}{2}}^{n+\frac{1}{2}} - \mathbf{G}_{i-\frac{1}{2}j-\frac{1}{2}}^{n+\frac{1}{2}} - \mathbf{G}_{i+\frac{1}{2}j-\frac{1}{2}}^{n+\frac{1}{2}}\right]. \quad (47)$$

After some algebraic manipulations, the complete scheme can be written in conservation form

$$\mathbf{Q}_{ij}^{n+1} = \mathbf{Q}_{ij}^{n} - \frac{\Delta t}{\Delta x}\left[\mathbf{F}_{i+\frac{1}{2}j} - \mathbf{F}_{i-\frac{1}{2}j} + \mathbf{G}_{ij+\frac{1}{2}} - \mathbf{G}_{ij-\frac{1}{2}}\right] \quad (48)$$

with numerical fluxes

$$\mathbf{F}_{i+\frac{1}{2}j} = \frac{1}{4}\left(\mathbf{F}_{i+\frac{1}{2}j-\frac{1}{2}}^{n+\frac{1}{2}} + \mathbf{F}_{i+\frac{1}{2}j+\frac{1}{2}}^{n+\frac{1}{2}}\right) + \frac{1}{16}\left(\mathbf{F}_{ij-1}^{n} + \mathbf{F}_{i+1j-1}^{n} - \frac{1}{2}\frac{\Delta x}{\Delta t}(\mathbf{Q}_{i+1j-1} - \mathbf{Q}_{ij-1})\right)$$
$$+ \frac{1}{16}\left(2\left(\mathbf{F}_{ij}^{n} + \mathbf{F}_{i+1j}^{n}\right) - 3\frac{\Delta x}{\Delta t}(\mathbf{Q}_{i+1j} - \mathbf{Q}_{ij})\right) + \frac{1}{16}\left(\mathbf{F}_{ij+1}^{n} + \mathbf{F}_{i+1j+1}^{n} - \frac{1}{2}\frac{\Delta x}{\Delta t}(\mathbf{Q}_{i+1j+1} - \mathbf{Q}_{ij+1})\right) \quad (49)$$

and

$$\mathbf{G}_{ij+\frac{1}{2}} = \frac{1}{4}\left(\mathbf{G}_{i+\frac{1}{2}j+\frac{1}{2}}^{n+\frac{1}{2}} + \mathbf{G}_{i-\frac{1}{2}j+\frac{1}{2}}^{n+\frac{1}{2}}\right) + \frac{1}{16}\left(\mathbf{G}_{i-1j}^{n} + \mathbf{G}_{i-1j+1}^{n} - \frac{1}{2}\frac{\Delta x}{\Delta t}(\mathbf{Q}_{i-1j+1} - \mathbf{Q}_{i-1j})\right)$$
$$+ \frac{1}{16}\left(2(\mathbf{G}_{ij}^{n} + \mathbf{G}_{ij+1}^{n}) - 3\frac{\Delta x}{\Delta t}(\mathbf{Q}_{ij+1} - \mathbf{Q}_{ij})\right) + \frac{1}{16}\left(\mathbf{G}_{i+1j}^{n} + \mathbf{G}_{i+1j+1}^{n} - \frac{1}{2}\frac{\Delta x}{\Delta t}(\mathbf{Q}_{i+1j+1} - \mathbf{Q}_{i+1j})\right). \quad (50)$$

In the Appendix we study the properties of the derived numerical schemes.

3.3. Comparison between first-order FORCEα and Rusanov fluxes

Now we show the behaviour of the proposed first-order FORCEα flux compared to the classical FORCE and Rusanov fluxes. For doing so we use the blast-wave interaction problem proposed by Woodward and Colella [44]. The initial condition consists of three constant states of an ideal gas with a ratio of specific heats given by $\gamma = 1.4$. This gas is at rest between reflecting walls separated by a distance of unity. The density is supposed to be $\rho = 1$ everywhere, while the initial pressure distribution is

$$p(x,0) = \begin{cases} 1000 & \text{if } 0 < x \leqslant 0.1, \\ 0.01 & \text{if } 0.1 < x \leqslant 0.9, \\ 100 & \text{if } 0.9 < x \leqslant 1.0. \end{cases} \quad (51)$$

In Fig. 3 we depict the solutions obtained using the classical Rusanov flux and FORCEα schemes, with $\alpha = 1$ (the classical FORCE scheme), $\alpha = 2$ and $\alpha = 3$ using 500 cells in the interval [0, 1]. The reference solution, also depicted, has been obtained by means of the Godunov flux with exact Riemann solver using 10,000 cells in the interval [0, 1], adapting the algorithm put forward in [42]. The output time is $t_{out} = 0.038$. Regarding the Courant number (CFL) we have taken for all fluxes 90% of their linear stability limit. This means CFL $= 0.9\frac{\sqrt{2\alpha-1}}{\alpha}$ (see the Appendix) for the FORCEα schemes and CFL $= 0.9$ for the Rusanov scheme.

The results obtained clearly show that when the number of space dimensions α increases, the first-order FORCEα fluxes become less diffusive than the classical FORCE flux and also than the Rusanov flux.

4. High order extensions

Once the first-order building block of the scheme has been set up and formulated as a two-point flux, as done in the previous sections, the high order extension in space and time is straightforward. In the finite volume framework, high order in
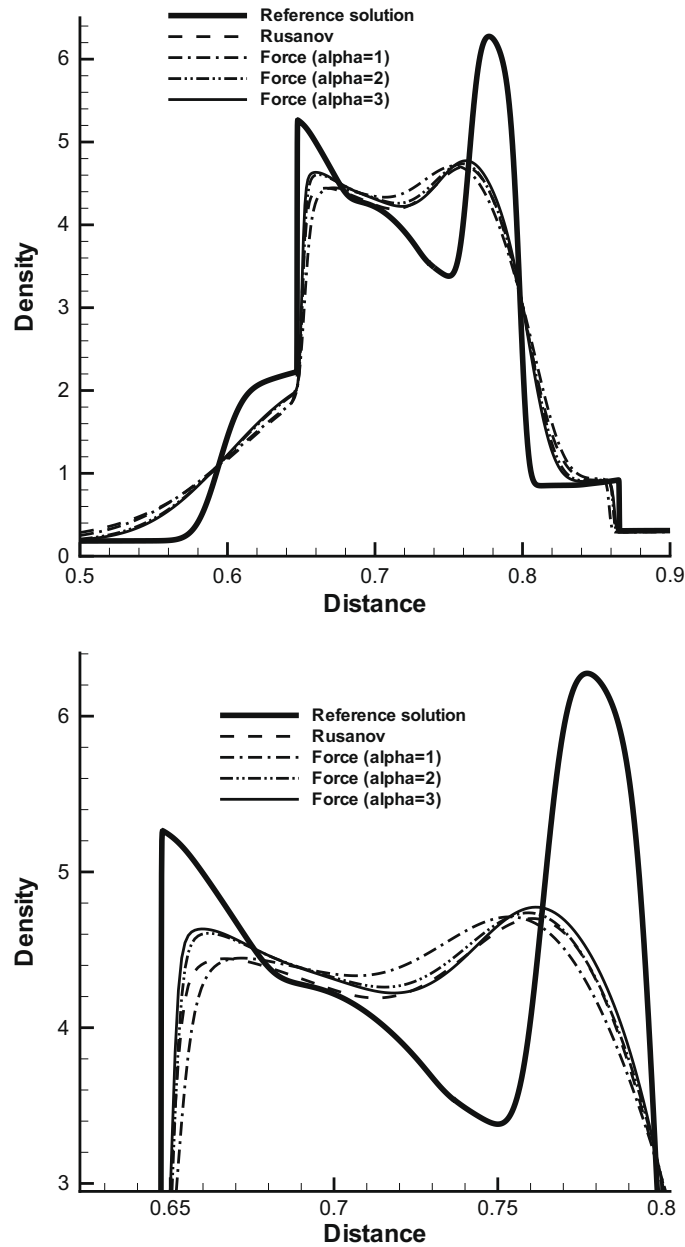
Fig. 3. Gas density for the 1D two-interactive blast waves problem to compare first-order Rusanov and FORCE-α fluxes ($\alpha = 1, 2, 3$) with 500 cells in [0, 1]. Reference solution obtained using Godunov flux with exact Riemann solver with 10,000 cells in [0, 1]. Output time $t_{out} = 0.0384$. The figure below is a zoom of the figure on top.

space is easily obtained using an ENO or WENO reconstruction procedure, see for example [23,27,1,39,26]. High order in space can be achieved either following the method-of-lines approach using TVD Runge–Kutta time discretizations [20], or a fully-discrete one-step approach as shown, e.g. in [23,40]. Recently, also the high order accurate discontinuous Galerkin schemes have received much attention for the solution of hyperbolic conservation laws, see, e.g. [7,9,8]. It is a particular feature of this discontinuous finite element approach that the boundary integral term is evaluated introducing a numerical flux function, where we also can directly apply our unstructured FORCE method as developed in this paper. In fact, we are convinced that it is a main key feature of the first-order version of our unstructured FORCE method that it can be cast into a two-point numerical flux, which can then be simply implemented in a straightforward manner in existing high order codes for hyperbolic conservation laws, using either the finite volume or the discontinuous Galerkin framework.

In this paper, we implement the unstructured FORCE flux in the unified framework of $P_N P_M$ schemes presented in [11] that contains fully-discrete one-step high order finite volume and discontinuous Galerkin finite element schemes as special

cases. In the case of finite volume schemes, the monotonicity is assured by a high order WENO reconstruction as presented in [12,13] for unstructured meshes in two and three space dimensions. A particular feature of the one-step $P_N P_M$ schemes is that they are completely quadrature-free at high order accuracy in space and time and thus they only need one non-linear flux evaluation per element face. The higher order terms are taken into account in a corrector flux, which, however, must be a linear function in its four arguments, see [12,11] for details. In the following applications, we use the unstructured FORCEα flux (34) as a leading flux and the unstructured Lax–Friedrichs-type flux (37) as a corrector flux.

4.1. Numerical convergence studies

The convergence studies of the two-dimensional high order extension of the proposed unstructured FORCE schemes are carried out solving the Euler equations of compressible gas dynamics, with conservative variables $\mathbf{Q} = (\rho, \rho v_j, \rho E)^T$ and the flux tensor defined as

$$\underline{\underline{\mathbf{F}}} = \begin{pmatrix} \rho v_i \\ \rho v_i v_j + p\,\delta_{ij} \\ v_i(\rho E + p) \end{pmatrix}. \tag{52}$$

To close the system we use the equation of state of a perfect gas

$$p = (\gamma - 1)\left(\rho E - \frac{1}{2}\rho(u^2 + v^2) \right). \tag{53}$$

We consider the smooth two-dimensional example of a convected isentropic vortex in a periodic computational domain $\Omega = [0; 10] \times [0; 10]$, given in detail for example in [26] or [13,11]. The initial condition is a linear superposition of a homogeneous background field and some perturbations δ:

$$(\rho, u, v, p) = (1 + \delta\rho, 1 + \delta u, 1 + \delta v, 1 + \delta p). \tag{54}$$

The perturbations of the velocity components u and v as well as the perturbations of entropy $S = \frac{p}{\rho^\gamma}$ and temperature T of the vortex are given by

$$\begin{pmatrix} \delta u \\ \delta v \end{pmatrix} = \frac{\epsilon}{2\pi} e^{\frac{1-r^2}{2}} \begin{pmatrix} -(y-5) \\ (x-5) \end{pmatrix}, \quad \delta S = 0, \quad \delta T = -\frac{(\gamma-1)\epsilon^2}{8\gamma\pi^2} e^{1-r^2} \tag{55}$$

with $r^2 = (x-5)^2 + (y-5)^2$, the vortex strength $\epsilon = 5$ and the ratio of specific heats $\gamma = 1.4$.

We use the sequence of irregular triangular meshes shown in Fig. 4 and set the Courant number to 0.7 of the maximum stability limit of the schemes. All computations are performed on one single CPU core of an Intel Core 2 Duo processor with 2.0 GHz clock speed and 2 GB of RAM. Computations are performed for a full period, i.e. until the final time $t = 10$, when the exact solution of the problem is given again by the initial condition.

We first run this test case for high order finite volume schemes from second to sixth order of accuracy in space and time, which are denoted as $P_0 P_M$ schemes in the general $P_N P_M$ framework. For comparison, we run the same test once with the new unstructured FORCE flux presented in this paper and with the classical Rusanov flux, as already done in [11], and the HLLE flux. The results are shown in Table 2. The L^2 error norms with the associated convergence rates for the density are presented. The first column of Table 2 entitled N_G characterizes the reciprocal mesh size and denotes the number of triangle edges used per space dimension. From Table 2 we conclude that for such smooth problems high order finite volume schemes seem to be more efficient than the low order version of the schemes. We also note that the unstructured FORCE flux gives slightly better error norms than the Rusanov scheme and in most cases is also slightly cheaper.

We then run this test case again using pure DG schemes ($P_N P_N$) from second to sixth order of accuracy in space and time and to conclude, we also put some representatives of the new general $P_N P_M$ class, namely a $P_2 P_3$ and a $P_3 P_5$ scheme of fourth
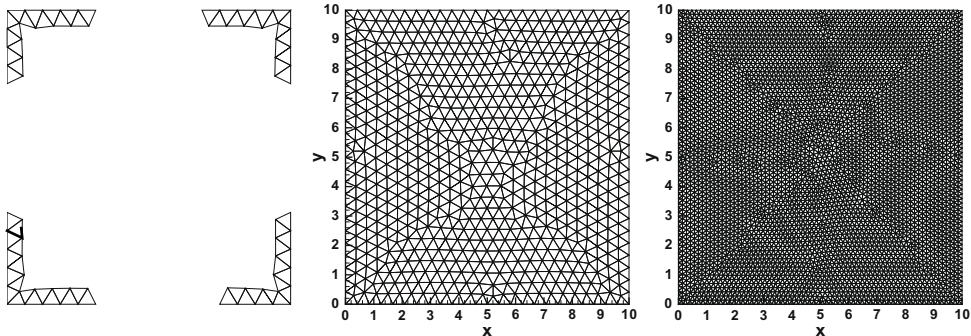
Table 2
Numerical convergence results obtained with P_0P_M finite volume schemes with the new unstructured FORCE flux (left), the Rusanov scheme (middle) and the HLLE flux (right). Second to sixth order in space and time.

	FORCE			Rusanov			HLLE		
N_G	L^2	$\mathcal{O}_{L^2}$	$t_{CPU}[s]$	L^2	$\mathcal{O}_{L^2}$	$t_{CPU}[s]$	L^2	$\mathcal{O}_{L^2}$	$t_{CPU}[s]$
$P_0P_1(\mathcal{O}2)$									
16	3.40E−01		1.0	3.87E−01		1.1	2.68E−01		1.1
32	1.06E−01	1.7	9.2	1.27E−01	1.6	9.0	7.84E−02	1.8	9.1
64	3.13E−02	1.8	67.6	3.78E−02	1.7	71.7	2.17E−02	1.9	72.3
128	9.08E−03	1.8	626.1	9.97E−03	1.9	659.7	5.31E−03	2.0	671.1
$P_0P_2(\mathcal{O}3)$									
16	3.04E−01		1.8	3.46E−01		1.9	2.47E−01		2.0
32	7.17E−02	2.1	14.5	8.67E−02	2.0	17.1	5.14E−02	2.3	15.3
64	1.35E−02	2.4	112.0	1.66E−02	2.4	120.0	9.91E−03	2.4	120.4
128	2.13E−03	2.7	1053	2.40E−03	2.8	1139	1.37E−03	2.9	1075
$P_0P_3(\mathcal{O}4)$									
16	7.01E−02		3.5	8.44E−02		3.5	5.89E−02		3.7
32	1.57E−02	2.2	27.8	1.91E−02	2.1	27.0	1.15E−02	2.4	27.5
64	1.10E−03	3.8	199.0	1.41E−03	3.8	207.5	8.27E−04	3.8	211.8
128	7.62E−05	3.8	1994	8.78E−05	4.0	1989	5.13E−05	4.0	1874
$P_0P_4(\mathcal{O}5)$									
16	6.41E−02		7.2	7.54E−02		6.8	5.32E−02		8.0
32	1.30E−02	2.3	50.0	1.58E−02	2.3	51.7	1.01E−02	2.4	54.8
64	6.62E−04	4.3	390.0	8.31E−04	4.2	397.7	5.18E−04	4.3	402.6
128	2.75E−05	4.6	3501	3.14E−05	4.7	3604	1.88E−05	4.8	3516
$P_0P_5(\mathcal{O}6)$									
16	4.79E−02		13.7	5.18E−02		13.5	5.27E−02		18.1
32	3.07E−03	4.0	108.3	3.56E−03	3.9	105.8	2.39E−03	4.5	113.7
64	8.73E−05	5.1	767.1	1.08E−04	5.0	783.4	6.58E−05	5.2	775.8
128	1.37E−06	6.0	6329	1.49E−06	6.2	6450	9.06E−07	6.2	6472

and sixth order of accuracy in space and time. We note that the two P_NP_M schemes are slightly more accurate and faster than the corresponding DG schemes at the same formal order of accuracy, see Table 3. More details on this topic can be found in [11].

5. Applications

Here we apply the high order version of the unstructured FORCE scheme of this paper to established test problems for the Euler and relativistic MHD equations.

5.1. Shock tube problems

5.1.1. 3D Euler equations

In this section we consider classical one-dimensional shock tube problems, but computed in a fully three-dimensional setting. We choose a computational domain $\Omega = [-0.5; 0.5] \times [-0.03; 0.03]^2$ with periodic boundary conditions in y and z

Table 3
Numerical convergence results obtained with high order one-step P_NP_M schemes using the new unstructured FORCE flux. Second to sixth order in space and time.

| N_G	L^2	$\mathcal{O}_{L^2}$	$t_{CPU}[s]$	L^2	$\mathcal{O}_{L^2}$	$t_{CPU}[s]$
	$P_1P_1(\mathcal{O}2)$			$P_2P_2(\mathcal{O}3)$		
16	6.10E−02		4.0	1.23E−02		11.9
24	2.47E−02	2.2	13.1	4.70E−03	2.4	43.9
32	1.11E−02	2.8	31.9	2.47E−03	2.2	92.5
64	2.16E−03	2.4	276.9	3.81E−04	2.7	740.8
	$P_2P_3(\mathcal{O}4)$			$P_3P_3(\mathcal{O}4)$		
16	3.52E−03		21.0	4.46E−03		33.7
24	7.21E−04	3.9	70.5	8.83E−04	4.0	108.8
32	2.08E−04	4.3	165.5	2.85E−04	3.9	256.8
64	1.31E−05	4.0	1287.7	1.91E−05	3.9	2013.0
	$P_3P_5(\mathcal{O}6)$			$P_5P_5(\mathcal{O}6)$		
16	2.11E−04		149.2	2.13E−04		259.8
24	2.07E−05	5.7	420.0	1.94E−05	5.9	734.5
32	3.66E−06	6.0	956.9	3.27E−06	6.2	1674.5
64	7.59E−08	5.6	6714.4	6.49E−08	5.7	11789.2
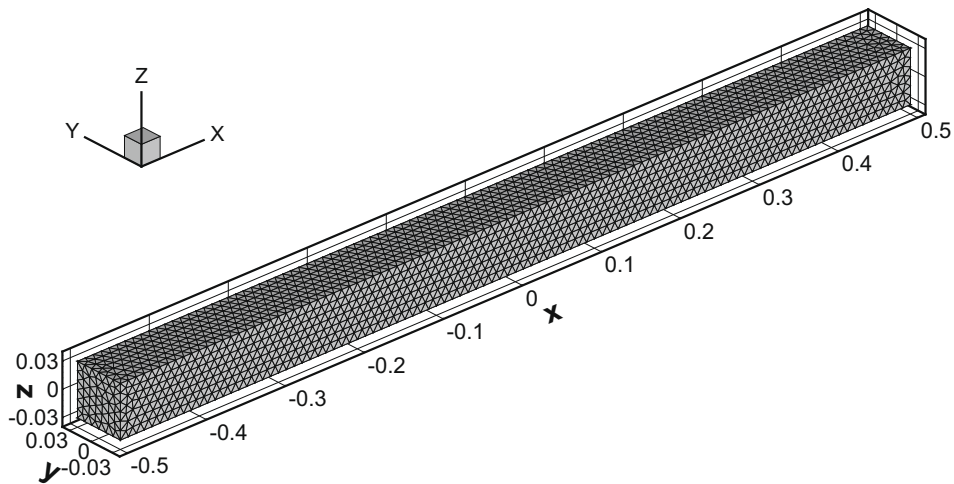
Fig. 5. Unstructured tetrahedral mesh used for the 3D shock tube problems.

Table 4
Initial states left and right and simulation end times for the 3D shock tube problems.

Test case	ρ_L	u_L	p_L	ρ_R	u_R	p_R	t_{end}
1	0.445	0.698	3.528	0.5	0.0	0.571	0.14
2	1.0	0.75	1.0	0.125	0.0	0.1	0.20
3	1.0	−2.0	0.4	1.0	2.0	0.4	0.15

direction and transmissive boundaries in x direction. The unstructured tetrahedral mesh used for our computations is depicted in Fig. 5 and contains 28,398 tetrahedral elements with a typical edge length of 0.01. This corresponds to an equivalent one-dimensional resolution of 100 cells. We solve the full three-dimensional Euler equations with $\gamma = 1.4$ using a third order (P_0P_2) WENO finite volume scheme [12,13,11] with the new unstructured FORCE flux presented in this paper. The initial condition is given by

$$(\rho, u, v, w, p)(\vec{x}, 0) = \begin{cases} (\rho_L, u_L, 0, 0, p_L) & \text{if } x < 0, \\ (\rho_R, u_R, 0, 0, p_R) & \text{if } x > 0. \end{cases} \tag{56}$$

The values of the left and right initial states for the various test cases are given in Table 4.

The first test case is known as the Lax shock tube problem and was proposed by Lax in [29] and is often computed in the research literature on high order WENO schemes. The second case corresponds to a modification of the standard Sod test case, proposed in [42]; this test contains a sonic point in the rarefaction fan that exposes entropy-violating schemes as well as some entropy-satisfying schemes via the well-known sonic glitch problem [34]. Test case 3 contains two very strong rarefaction waves that generate a low density region in the middle of the computational domain; this test is also known and the 123 problem.

The results depicted in Fig. 6 show the solution for density ρ and pressure p on 100 equidistant sample points taken on the x-axis ($y = z = 0$) at the final output times t_{end} given in Table 4. For all test cases we note a very good agreement with the exact reference solution.

5.1.2. 2D relativistic MHD equations

The relativistic MHD (RMHD) equations form a very complicated hyperbolic system. Particular complications arise from the fact that the primitive variables, which enter the physical flux, can not be expressed any more in a closed analytical form in terms of the conserved quantities. The details about this very interesting hyperbolic system can be found in [3,45,15,24,36]. For the multi-dimensional version of the equations, we enforce the divergence-free condition of the magnetic field using the hyperbolic divergence-cleaning approach proposed by Dedner et al. [10] setting the divergence cleaning speed equal to unity. We use the notation of [45], except for the momentum vector, which we call M_j in this paper. The vector of conserved variables $\mathbf{Q}$ is then given in terms of the primitive variables ρ, v_j, p, B_j and Ψ by

$$\mathbf{Q} = \begin{pmatrix} D \\ M_j \\ E \\ B_j \\ \Psi \end{pmatrix} = \begin{pmatrix} \gamma\rho \\ \gamma w_{\text{tot}} v_j - b^0 b^j \\ \gamma^2 w_{\text{tot}} - b^0 b^0 - p_{\text{tot}} \\ B_j \\ \Psi \end{pmatrix}. \tag{57}$$
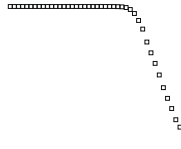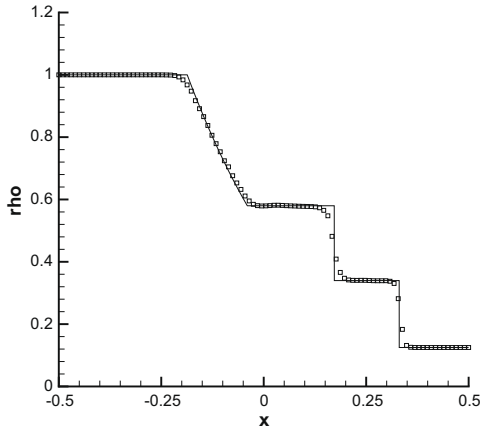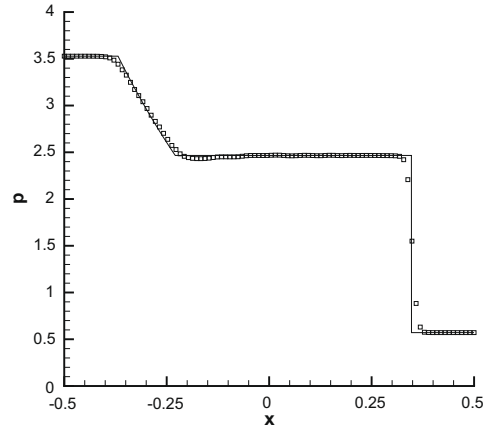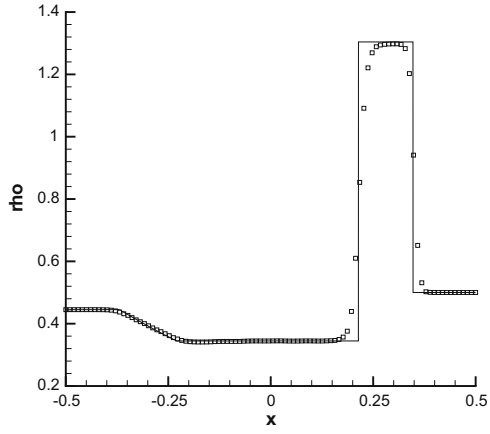
The flux tensor is defined in multiple space dimensions as

$$
\underline{\underline{\mathbf{F}}} = \begin{pmatrix} \gamma \rho \, v_i, \\ \gamma^2 w_{\text{tot}} \, v_i v_j - b^i b^j + p_{\text{tot}} \delta_{ij}, \\ \gamma^2 w_{\text{tot}} \, v_i - b^0 b^i \\ v_i B_j - B_i v_j + \Psi \delta_{ij} \\ c_h^2 B_i \end{pmatrix}.
$$
(58)

The equation of state is

$$e = \rho + \frac{p}{\Gamma - 1},$$

(59)

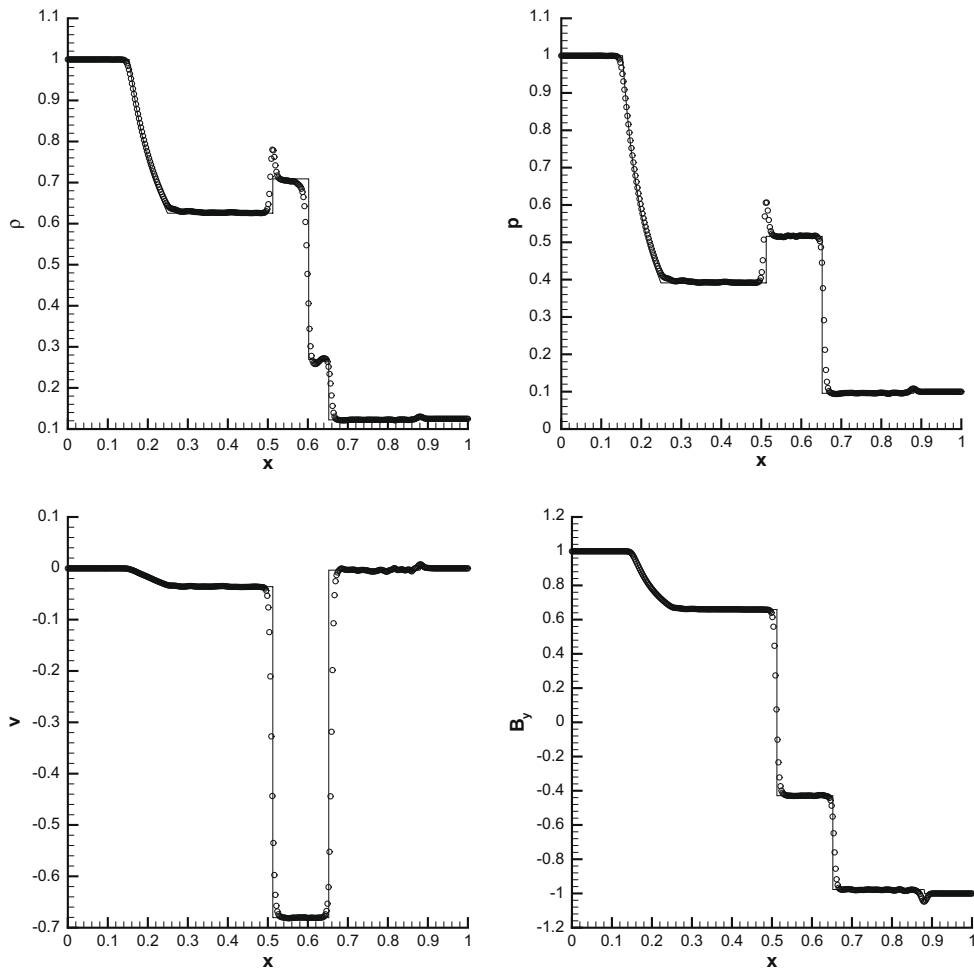the Lorentz factor, denoted as γ in this section, is defined by

$$\gamma = \frac{1}{\sqrt{1 - \vec{v}^2}},$$

(60)

and further quantities appearing in (57) and (58) are given by

$$b^0 = \gamma v_k B_k, \quad b^i = \frac{B_i}{\gamma} + \gamma v_i (v_k B_k), \quad |b|^2 = \frac{\vec{B}^2}{\gamma^2} + (v_k B_k)^2,$$

(61)

Table 5
Initial states left (L) and right (R) for the RMHD shock tubes with final times t_e.

Case	ρ	p	u	v	w	B_y	B_z	B_x	t_e
1 L	1.0	1.0	0.0	0.0	0.0	1.0	0.0	0.5	0.4
1 R	0.125	0.1	0.0	0.0	0.0	−1.0	0.0	0.5	
2 L	1.08	0.95	0.4	0.3	0.2	0.3	0.3	2.0	0.55
2 R	1.0	1.0	−0.45	−0.2	0.2	−0.7	0.5	2.0	

Fig. 7. Results for the RMHD Riemann problem 1 at $t = 0.4$ computed in 2D on 17,628 triangles. $P_0 P_2$ WENO scheme (circles) and exact reference solution [15].

from which total enthalpy and total pressure are then finally defined as

$$w_{\text{tot}} = e + p + |b|^2, \quad p_{\text{tot}} = p + \frac{1}{2}|b|^2. \tag{62}$$

In this entire section, the speed of light is supposed to be set to unity. The computation of the primitive variables ρ, v_k and p from the vector u_p of conserved quantities is very complicated. It can not be done analytically but requires necessarily the use of an iterative technique such as Newton's method. A very elegant, robust and efficient way of transforming the conservative variables to primitive variables using the analytic inversion of a third degree polynomial together with one non-linear scalar equation to which subsequently Newton's method is applied is given in [45].

As in [11] we solve the two-dimensional version of two standard shock tube test cases proposed originally in one space dimension in [3]. The initial condition consists of two piece-wise constant states on the left and the right of the discontinuity located at $x = 0.5$. The initial states are summarized in Table 5. In test case 1 we use $\Gamma = 2$ and in the second one we use $\Gamma = 5/3$, according to [3]. We solve these test cases in the computational domain $\Omega = [0;1] \times [0;0.05]$ on an unstructured triangular mesh consisting of 17,628 elements in two space dimensions, corresponding to an equivalent one-dimensional resolution of 400 points. We apply periodic boundary conditions in y-direction and transmissive boundaries in x-direction. The shock capturing is again achieved via the unstructured WENO reconstruction procedure described in [12,13]. A cut through the computational results at $y = 0.025$ is shown in Figs. 7 and 8 and a 3D visualization of the solution together with the mesh is depicted in Fig. 9.

5.2. Two-dimensional explosion problem

Here, we solve a strong two-dimensional explosion test problem in a circular computational domain Ω with radius $R = 1$ using again a third order WENO finite volume scheme with the new unstructured FORCE flux as building block on an
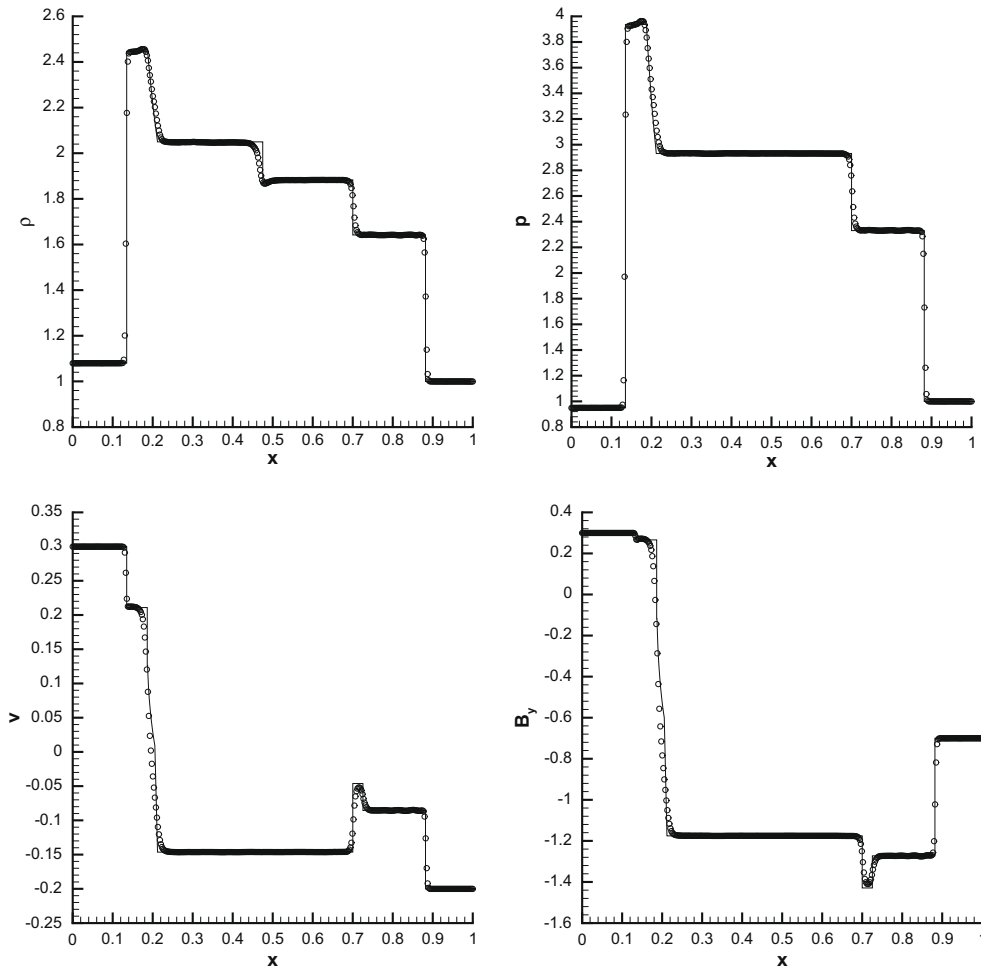

Fig. 8. Results for the RMHD Riemann problem 2 at $t = 0.55$ computed in 2D on 17,628 triangles. P_0P_2 WENO scheme (circles) and exact reference solution [15].
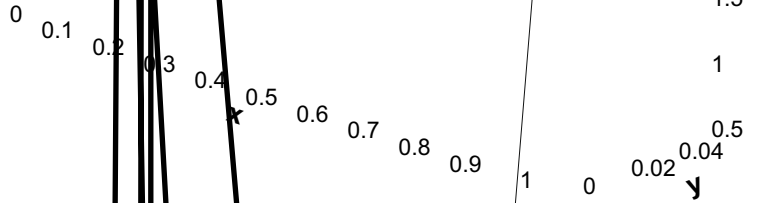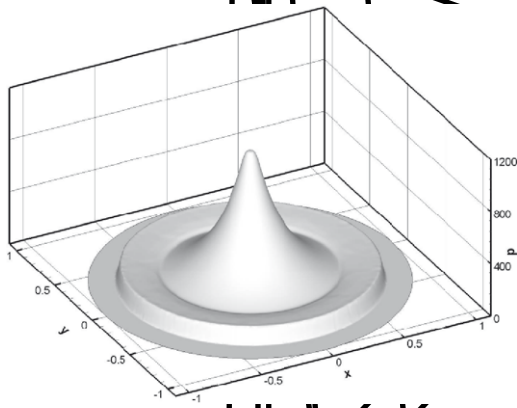
Figure 9: Results of the 2D explosion test problem at time $t = 0.03$ using a P_0P_2 scheme with the new FORCE flux on an unstructured triangular mesh. (a) 2D pressure distribution, (b) density, (c) velocity and (d) pressure shown on a cut along the x-axis.

unstructured triangular mesh with 100,970 triangles. The governing equations are the two-dimensional Euler equations with $\gamma = 1.4$. The initial condition is given by

$$(\rho, u, v, w, p)(\vec{x}, 0) = \begin{cases} (10, 0, 0, 0, 1000) & \text{if } r < 0.4, \\ (1, 0, 0, 0, 0.1) & \text{if } r > 0.4, \end{cases} \tag{63}$$

with $r^2 = x^2 + y^2$. The pressure jumps over four orders of magnitude and thus will produce a very strong outward traveling shock wave. The reference solution is computed using the symmetry of the problem in angular direction solving an equivalent one-dimensional hyperbolic PDE with source terms on a very fine mesh (10,000 cells) using a second-order TVD scheme, see [42] for details. A total view of the solution is given in Fig. 10(a) and one-dimensional cuts through the solution along the x-axis are shown in Fig. 10(b)–(d) are shown for density, radial velocity and pressure. The presented third order computation with the new unstructured FORCE flux on the unstructured two-dimensional mesh agrees very well with the reference solution.

5.3. Double Mach reflection problem

In this section we consider a very well-known test case with reflecting wall boundary conditions, the so-called double Mach reflection problem, originally proposed by Woodward and Colella in [44]. It exhibits very strong discontinuities, wall-bounded flows and furthermore develops rich small-scale structures in time, which are difficult to resolve. The governing equations are still the two-dimensional Euler equations with $\gamma = 1.4$. The test consists in a moving shock wave (shock Mach number $M_s = 10$) that hits a 30° ramp. The initial condition for this problem is given by the Rankine–Hugoniot conditions as follows:

$$(\rho, u, v, p)(\vec{x}, 0) = \begin{cases} (8.0, 8.25, 0.0, 116.5) & \text{if } x < 0.1, \\ (1.4, 0.0, 0.0, 1.0) & \text{if } x \geqslant 0.1. \end{cases} \tag{64}$$

Due to the unstructured formulation of the scheme, we compute the problem directly in its original physical setup, as proposed in [38] for block-structured meshes and in [13] for unstructured triangular meshes. We solve the problem with
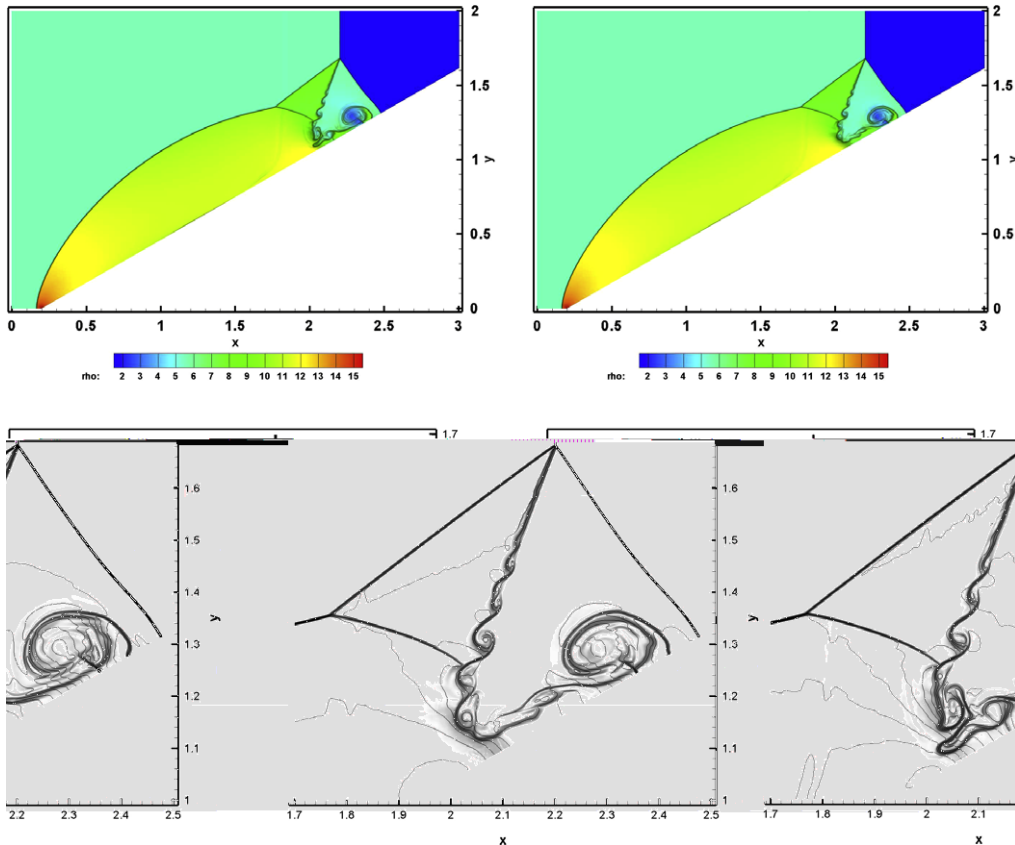

Fig. 11. Results obtained for the Double Mach Reflection Problem at $t = 0.21$ with the P_0P_2 scheme. A mesh with $h = 1/800$ has been used. Left column: the new unstructured FORCE flux. Right column: the classical Rusanov flux.

a third order P_0P_2 WENO finite volume scheme using the unstructured FORCE flux proposed in this article as well as the classical Rusanov flux for comparison purposes. We use a characteristic triangular mesh spacing of $h = 1/800$, leading to 5,456,906 triangles. Solid wall boundary conditions are imposed on the ramp and on the upper boundary ($y = 2$). Our results obtained at $t = 0.21$ for the density (31 equidistant contour levels from 1.5 to 21.5) are depicted in Fig. 11. The contour lines agree qualitatively with the results shown in previous publications on this test problem [4,26,27,40,13].

6. Concluding remarks

A generalization of the one-dimensional FORCE flux to multiple space dimensions for solving hyperbolic equations in conservation-law form on general meshes has been presented. Monotonicity, linear stability and numerical viscosity of the schemes have been analyzed for the case of structured meshes in two and three space dimensions. We have then extended the new FORCE fluxes to high order of accuracy in space and time in the framework and finite volume and discontinuous Galerkin finite element methods. Results for schemes of up to sixth order of accuracy in space and time on unstructured meshes have been shown. For smooth solutions the convergence rates of the schemes have been analyzed and compared with that of Godunov-type methods with the simple Riemann solvers of Rusanov and HLLE; errors and CPU times have also been compared. For shocked flows the performance of the numerical schemes has been assessed by solving some well-established test problems for the Euler and relativistic MHD equations on unstructured meshes. The main feature of the proposed schemes is simplicity; it does not require explicit knowledge of the eigenstructure of the system, nor the availability of a Riemann solver. This is attractive for very complex hyperbolic systems, for which a Riemann solver may not be available, or if available it might not be suitable. Generality is the other main feature of the new FORCE schemes; no matter how complicated the equations are, provided they are written in conservation-law form, the schemes of this paper are readily applicable. Finally we note that the proposed FORCE schemes can be extended to high order of accuracy in space and time in a straight forward manner and can be incorporated in any existing finite volume or DG finite element solver. This is possible since the first-order FORCE method can be cast into a one-step flux-conservative form whose numerical fluxes only depend on the left and right state at the edge.

Ongoing research on this topic concerns the extension of the unstructured FORCE schemes to non-linear systems of non-conservative hyperbolic systems. Preliminary results of the authors indicate that this is possible.

Appendix A. Properties of the FORCE scheme on edge-based secondary volumes

Here we study monotonicity, linear stability and numerical viscosity of the schemes. The study is based on the linear advection equation with constant coefficients, in two and three space dimensions

$$\partial_t q + \partial_x f(q) + \partial_y g(q) + \partial_z h(q) = 0 \tag{65}$$

with the fluxes $f(q) = \lambda_1 q, g(q) = \lambda_2 q$ and $h(q) = \lambda_3 q$.

We first study the multi-dimensional version (38) of the GFORCEα schemes. The GFORCEα fluxes on Cartesian meshes contain the two parameters ω and α, where α is the number of space dimensions and $0 \leqslant \omega \leqslant 1$ is a weight.

The numerical scheme for Eq. (65) is written as

$$q_{i,j,k}^{n+1} = q_{i,j,k}^n - \frac{\Delta t}{\Delta x}\left(f_{i+\frac{1}{2},j,k} - f_{i-\frac{1}{2},j,k}\right) - \frac{\Delta t}{\Delta y}\left(g_{i,j+\frac{1}{2},k} - g_{i,j-\frac{1}{2},k}\right) - \frac{\Delta t}{\Delta z}\left(h_{i,j,k+\frac{1}{2}} - h_{i,j,k-\frac{1}{2}}\right), \tag{66}$$

where, as an example, we give the expression of the numerical flux in x direction

$$f_{i+\frac{1}{2},j,k} = \frac{\lambda_1}{2}\left(q_{i,j,k}^n + q_{i+1,j,k}^n\right) - \frac{\lambda_1}{2\alpha c_x}\left[\omega(\alpha^2 c_x^2 - 1) + 1\right]\left(q_{i+1,j,k}^n - q_{i,j,k}^n\right), \tag{67}$$

with directional Courant number $c_x = \frac{\lambda_1 \Delta t}{\Delta x}$. The numerical scheme reads

$$q_{i,j,k}^{n+1} = \sum_{l=-1}^{1}\sum_{m=-1}^{1}\sum_{r=-1}^{1}\beta_{l,m,r} q_{i+l,j+m,k+r}^n \tag{68}$$

with coefficients

$$\beta_{-1,0,0} = \frac{1+\alpha c_x}{2\alpha} - \omega\left(\frac{1-\alpha^2 c_x^2}{2\alpha}\right), \quad \beta_{1,0,0} = \frac{1-\alpha c_x}{2\alpha} - \omega\left(\frac{1-\alpha^2 c_x^2}{2\alpha}\right),$$

$$\beta_{0,-1,0} = \frac{1+\alpha c_y}{2\alpha} - \omega\left(\frac{1-\alpha^2 c_y^2}{2\alpha}\right), \quad \beta_{0,1,0} = \frac{1-\alpha c_y}{2\alpha} - \omega\left(\frac{1-\alpha^2 c_y^2}{2\alpha}\right),$$

$$\beta_{0,0,-1} = \frac{1+\alpha c_z}{2\alpha} - \omega\left(\frac{1-\alpha^2 c_z^2}{2\alpha}\right), \quad \beta_{0,0,1} = \frac{1-\alpha c_z}{2\alpha} - \omega\left(\frac{1-\alpha^2 c_z^2}{2\alpha}\right),$$

$$\beta_{0,0,0} = \omega\left(1 - \alpha c_x^2 - \alpha c_y^2 - \alpha c_z^2\right). \tag{69}$$

The monotonicity regions of the schemes are established from (68) and (69) by requiring that the coefficients be non-negative. The results obtained are summarized in Table 6 and note that the monotonicity regions coincide with the linear stability regions.

We analyze the linear stability of the schemes by means of the von Neumann method. For the one-dimensional case, but keeping the dimension α as a parameter we obtain the following linear stability region

$$|c| \leqslant \begin{cases} \sqrt{\frac{-1+\omega}{\alpha(\omega\alpha-1)}} & \text{if } 0 \leqslant \omega < \frac{1}{\alpha+1}, \\ \frac{1}{\omega\alpha}\sqrt{\omega(\omega+\alpha-1)} & \text{if } \frac{1}{\alpha+1} \leqslant \omega \leqslant 1. \end{cases} \tag{70}$$

For the special case $\omega = \frac{1}{2}$ the stability condition is

$$|c| \leqslant \frac{\sqrt{2\alpha-1}}{\alpha}, \tag{71}$$

which coincides with the monotonicity condition, see Table 6. This interesting property does not hold when $\omega \neq \frac{1}{2}$; that is the schemes are not monotone in the whole linear stability range. It is easy to verify that the condition contains the well-known special cases $\omega = \frac{1}{2}, \alpha = 1$ (classical FORCE), $\omega = 1, \alpha = 1$ (the Lax–Wendroff scheme) and $\omega = 0, \alpha = 1$ (Lax–Friedrichs scheme), see Table 1.

For the two and three-dimensional cases we use the numerical technique reported in [43] to obtain an indication of the linear stability region of the scheme. Fig. 12 shows the results in the $c_x - c_y$ for the two-dimensional case (left) and the three-dimensional one (right). Here the region of linear stability coincides with the region of monotonicity given in Table 6 for the case $\omega = \frac{1}{2}$.

Regarding the numerical viscosity of the schemes we first consider the one-dimensional case, with the dimension α left as a parameter. The numerical viscosity has the expression

$$\mu = \frac{1}{2\alpha}(1 - \omega + \omega\alpha^2 c^2)\frac{\Delta x^2}{\Delta t} - \frac{1}{2}\lambda^2\Delta t, \tag{72}$$

which for $\omega = \frac{1}{2}$ in (72) gives

$$\mu = \frac{\Delta x^2}{\Delta t}\frac{1}{4\alpha} + \frac{\lambda^2}{2}\Delta t(\alpha - 2). \tag{73}$$

We note that the numerical viscosity is an increasing function of the dimension α. However, for low speeds of propagation, the numerical viscosity decreases as α increases. Note that for $\alpha = 2$ the numerical viscosity does not depend on the speed λ.
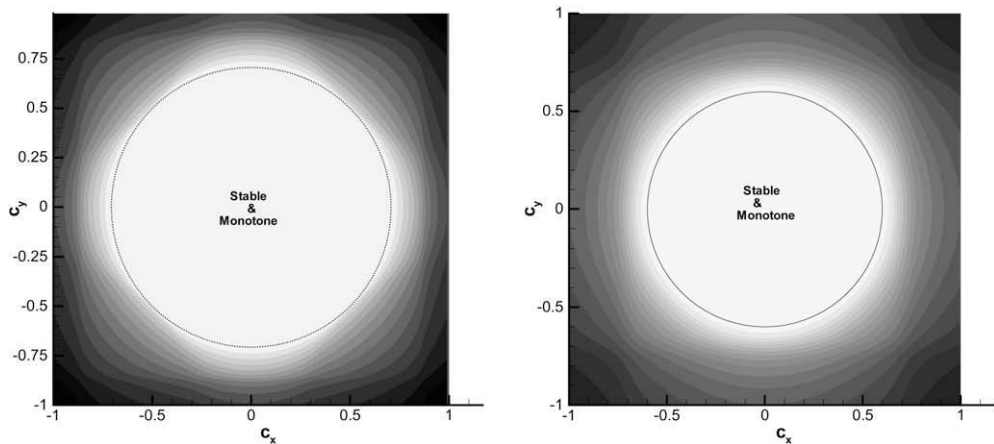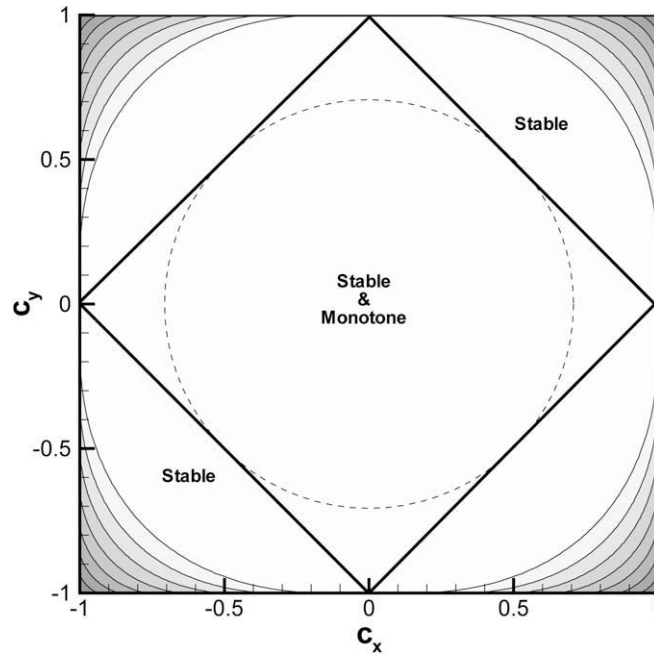

Fig. 12. Linear stability regions for the multi-dimensional FORCE schemes. Left picture depicts the two-dimensional case in the $c_x - c_y$ plane. The right picture shows a cut through the stability region in the $c_x - c_y$ plane for the three-dimensional case.

Table 6
Monotonicity regions for the numerical schemes in one, two and three space dimensions, as function of the Courant number c and the weighting parameter ω. In the one-dimensional case the dimension α is also left as a parameter.

ω	1D	2D	3D
$0 \leqslant \omega < \frac{1}{2}$	$|c| \leqslant \frac{1}{\alpha}$	$|c_x|, |c_y| \leqslant \frac{1}{2}$	$|c_x|, |c_y|, |c_z| \leqslant \frac{1}{3}$
$\omega = \frac{1}{2}$	$|c| \leqslant \frac{\sqrt{2\alpha-1}}{\alpha}$	$c_x^2 + c_y^2 \leqslant \frac{1}{2}$	$c_x^2 + c_y^2 + c_z^2 \leqslant \frac{1}{3}$
$\frac{1}{2} < \omega < 1$	$|c| \leqslant |\frac{-1+\omega}{\omega\alpha}|$	$|c_x|, |c_y| \leqslant |\frac{-1+\omega}{2\omega}|$	$|c_x|, |c_y|, |c_z| \leqslant |\frac{-1+\omega}{3\omega}|$

Fig. 13. Linear stability and monotonicity regions for the two-dimensional FORCE scheme on vertex-based secondary volumes (square in full line). Also shown are the stability and monotonicity regions for the two-dimensional FORCE scheme on edge-based secondary volumes (circle in dotted line).

Expression (72) allows us to compute the numerical viscosity in multi-dimensional schemes in the Cartesian directions x, y, z, by just setting α to the appropriate value. Note that in the multi-dimensional case there is numerical viscosity in the transversal direction. In the two-dimensional case we have

$$\mu_{xy} = -\lambda_1 \lambda_2 \Delta t, \tag{74}$$

and in the three-dimensional case the numerical viscosities in transversal directions are

$$\mu_{xy} = -\lambda_1 \lambda_2 \Delta t, \quad \mu_{xz} = -\lambda_1 \lambda_3 \Delta t, \quad \mu_{yz} = -\lambda_2 \lambda_3 \Delta t. \tag{75}$$

Appendix B. Properties of the FORCE scheme on vertex-based secondary volumes

Here we study the properties of the FORCE schemes using vertex-based secondary volumes. For the two-dimensional case the stencil is identical to that used by Jiang–Tadmor [28] for their second-order schemes. The monotonicity region is given by the following conditions:

$$c_x + c_y \leqslant 1, \tag{76}$$
$$|c_x - c_y| \leqslant 1, \tag{77}$$

and

$$c_x^2 + c_y^2 \leqslant 1. \tag{78}$$

The most restrictive constraints are (76) and (77), which results in a squared region in the $c_x - c_y$ plane, centred at $(0, 0)$. Restriction (78) is a circle of radius $r = 1$ and centre $(0, 0)$. Fig. 13 shows the linear stability and monotonicity regions for the scheme. The FORCE scheme based on the Jiang–Tadmor stencil has a monotonicity region (square in full line) that is smaller than its linear stability region (the outer circle). Also shown in Fig. 13 are the stability and monotonicity regions for the two-dimensional FORCE scheme on edge-based secondary volumes (circle in dotted line); as said earlier here the stability and monotonicity regions coincide, and are smaller than the monotonicity region of the FORCE schemes on vertex-based secondary volumes, the Jiang–Tadmor stencil.

The numerical viscosity of the FORCE schemes on vertex-based secondary volumes, the Jiang–Tadmor stencil, has numerical viscosity

$$\mu_x = \frac{1}{4}(1 - c_x^2)\frac{\Delta x^2}{\Delta t}, \quad \mu_y = \frac{1}{4}(1 - c_y^2)\frac{\Delta y^2}{\Delta t}, \quad \mu_{xy} = 0. \tag{79}$$

References

[1] R. Abgrall, On essentially non-oscillatory schemes on unstructured meshes: analysis and implementation, Journal of Computational Physics 144 (1994) 45–58.

[2] P. Arminjon, A. St-Cyr, Nessyahu–Tadmor-type central finite volume methods without predictor for 3D Cartesian and unstructured tetrahedral grids, Applied Numerical Mathematics 46 (2003) 135–155.

[3] D. Balsara, Total variation diminishing scheme for relativistic magnetohydrodynamics, The Astrophysical Journal Supplement Series 132 (2001) 83–101.

[4] D. Balsara, C.W. Shu, Monotonicity preserving weighted essentially non-oscillatory schemes with increasingly high order of accuracy, Journal of Computational Physics 160 (2000) 405–452.

[5] F. Bianco, G. Puppo, G. Russo, High order central schemes for hyperbolic systems of conservation laws, SIAM Journal on Scientific Computing 21 (1999) 294–322.

[6] G.Q. Chen, E.F. Toro, Centred difference schemes for nonlinear hyperbolic equations, Journal of Hyperbolic Differential Equations 1 (2004) 531–566.

[7] B. Cockburn, S. Hou, C.W. Shu, The Runge–Kutta local projection discontinuous Galerkin finite element method for conservation laws IV: the multidimensional case, Mathematics of Computation 54 (1990) 545–581.

[8] B. Cockburn, G.E. Karniadakis, C.W. Shu, Discontinuous Galerkin Methods, Lecture Notes in Computational Science and Engineering, Springer, 2000.

[9] B. Cockburn, C.W. Shu, The Runge–Kutta discontinuous Galerkin method for conservation laws V: multidimensional systems, Journal of Computational Physics 141 (1998) 199–224.

[10] A. Dedner, F. Kemm, D. Kröner, C.-D. Munz, T. Schnitzer, M. Wesenberg, Hyperbolic divergence cleaning for the MHD equations, Journal of Computational Physics 175 (2002) 645–673.

[11] M. Dumbser, D. Balsara, E.F. Toro, C.D. Munz, A unified framework for the construction of one-step finite-volume and discontinuous Galerkin schemes, Journal of Computational Physics 227 (2008) 8209–8253.

[12] M. Dumbser, M. Käser, Arbitrary high order non-oscillatory finite volume schemes on unstructured meshes for linear hyperbolic systems, Journal of Computational Physics 221 (2007) 693–723.

[13] M. Dumbser, M. Käser, V. A Titarev, E.F. Toro, Quadrature-free non-oscillatory finite volume schemes on unstructured meshes for nonlinear hyperbolic systems, Journal of Computational Physics 226 (2007) 204–243.

[14] M. Dumbser, M. Käser, E.F. Toro, An arbitrary high order discontinuous Galerkin method for elastic waves on unstructured meshes V: Local time stepping and p-adaptivity, Geophysical Journal International 171 (2007) 695–717.

[15] B. Giacomazzo, L. Rezzolla, The exact solution of the Riemann problem in relativistic magnetohydrodynamics, Journal of Fluid Mechanics 562 (2006) 223–259.

[16] J. Glimm, Solution in the large for nonlinear hyperbolic systems of equations, Communications on Pure Applied Mathmatics 18 (1965) 697–715.

[17] E. Godlewski, P.A. Raviart, Numerical Approximation of Hyperbolic Systems of Conservation Laws, Springer, 1996.

[18] S.K. Godunov, A.V. Zabrodin, G.P. Prokopov, A difference scheme for two-dimensional unsteady aerodynamics, Journal of Computational Mathematics and Mathematical Physics USSR 2 (6) (1961) 1020–1050.

[19] S.K. Godunov, Finite difference methods for the computation of discontinuous solutions of the equations of fluid dynamics, Mathematics of the USSR-Sbornik 47 (1959) 271–306.

[20] S. Gottlieb, C.W. Shu, Total variation diminishing Runge–Kutta schemes, Mathematics of Computation 67 (1998) 73–85.

[21] B. Haasdonk, D. Kröner, C. Rohde, Convergence of a staggered-Lax–Friedrichs-scheme on unstructured grids in 2d, Numerische Mathematik 88 (2001) 459–484.

[22] A. Harten, High resolution schemes for hyperbolic conservation laws, Journal of Computational Physics 49 (1983) 357–393.

[23] A. Harten, B. Engquist, S. Osher, S.R. Chakravarthy, Uniformly high order accurate essentially non-oscillatory schemes III, Journal of Computational Physics 71 (1987) 231–303.

[24] V. Honkkila, P. Janhunen, HLLC solver for ideal relativistic MHD, Journal of Computational Physics 223 (2007) 643–656.

ik3554–393.

(1u15abrten, B. En3r, P..372grB68(S.)-Wendroffntiallymics,accurate essentiallyervation La368(i324(Springer,M-34tions)-431(1996.)])-27ids in of603(88)-5(21,)-27t